PROCEEDINGS
OF THE
NATIONAL ACADEMY OF SCIENCES
Volume 19 February 15, 1933 Number 2

THE NEWTON-DENNING METHOD FOR COMPUTING METEOR PATHS WITH A CELESTIAL GLOBE

By Willard J. Fisher

Harvard College Observatory

Communicated January 11, 1933

Partial methods for the computation of meteor paths with the help of the celestial globe have been given by Newton[1] and Denning.[2] In connection with the reduction of certain fireball observations the writer has combined these two methods for the special case of two observers only. Newton gives details of a globe reduction for a Leonid fireball with numerous observers, and with many ingenious devices for the use of varied data. Denning is nowhere so full; and in fact, it is not known to the writer whether he ever varied and extended his method.

The globe available to the writer is marked, Edinburgh, 1879, and has a wooden horizon, a brass meridian and a brass strap altitude arc. The circles are easily brought into adjustment within a quarter degree or better, and the error of the altitude arc is nearly constant throughout; but the map gores are pasted on the ball with a lower degree of accuracy, so that errors of a degree in final readings must be expected quite frequently. As most fireball data are relatively good if accurate within a degree, such a globe may be tolerated for fireball reductions. The trigonometric work depending on angles and arcs so computed is done with superfluous accuracy with the help of a ten inch slide rule.

Observers at two points on the ground, P_1 and P_2 (Fig. *A*) see a meteor, M, shoot in a straight line through the atmosphere from a to b. O' is a point on the ground halfway between P_1 and P_2. A plane is passed through P_1 and P_2, parallel to a plane passed through O' tangent to the earth's surface. Prolonged forward and downward the meteor path cuts this plane at O''.

The celestial sphere (Fig. *B*) is oriented for the mean latitude of P_1 and P_2, and for the mean sidereal time of observation. With regard to this sphere the plane triangle $P_1O''P_2$ is infinitesimal, and may be considered as concentrated in the point O, the center of the sphere. The plane of this triangle contains the celestial horizon, except for the minute error

due to the differences in sea height of P_1 and P_2. The line P_1P_2 prolonged both ways cuts the celestial sphere in the horizon at P_1' and P_2'. P_1O'' prolonged, and P_2O'' prolonged, meet the horizon in E_1 and E_2, respectively. The horizon arc E_1E_2 measures the angle $P_1O''P_2$ of the plane triangle. (Newton does not mention these horizon points.)

The meteor path, ab, or M, produced backward meets the celestial sphere in the radiant, R. The meteor path, ab, projected on the sphere, as seen from P_1, is a great circle arc M_1 or a_1b_1, and as seen from P_2 is a great circle arc M_2 or a_2b_2. These two arcs prolonged backward intersect each other in R; prolonged forward, they intersect the horizon in E_1 and E_2.

a, being any point on the meteor path M, its projections on the sphere,

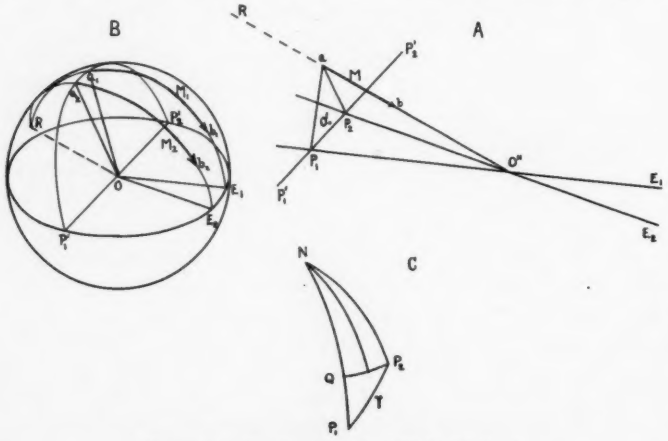

Geometry, Newton-Denning Globe Method.

as seen from P_1 and P_2, are a_1 and a_2. Then the points P_1', a_2, a_1, P_2', lie on an arc of a great circle. (Denning does not mention this circle.) And any great circle through P_1' and P_2', which cuts M_1 and M_2 on the sky, thereby marks two points on the projected meteor paths, which correspond to a single point on the real meteor path.

The plane triangle P_1aP_2 (Fig. A) is in the plane of the great circle $P_1'a_2a_1P_2'$ (Fig. B), and the angles of the plane triangle are measured by arcs of the great circle. Measuring these arcs on the globe, and the base P_1P_2 on the ground, the plane triangle may be solved for the sides P_1a and P_2a (a step used by Newton).

Also, arcs of the great circle $Ra_1b_1E_1$ measure angles of the plane triangle $P_1O''a$. Thus, E_1b_1R measures the supplement of the angle $P_1O''a$, and $E_1b_1a_1$ measures the angle $O''P_1a$; so that, knowing P_1a from the previous

triangle, P_1O'' may be computed; similarly, for arc $Ra_2b_2E_2$ and plane triangle $P_2O''a$.

The point O'' may also be computed by plotting or trigonometry, with P_1 and P_2 given and E_1 and E_2 measured.

The altitude and azimuth of the radiant R (Fig. B) are its altitude and azimuth as seen from O'' (Fig. A), which is a point above the earth's surface; or from O', under favorable conditions.

The vertical great circle through R is in the vertical plane of the meteor's motion, with regard to the horizon of O', and as seen from O''.

The inclination of the plane P_1aP_2 (Fig. A) to the horizon plane is the inclination of the great circle $P_1'a_2a_1P'$ (Fig. B) to the horizon. This inclination being measured on the globe, the actual height of a above the horizon plane of O' may be computed. The perpendicular from a to the base $P_1P_2 = P_1P_2 \dfrac{\sin P_1 \sin P_2}{\sin(P_1 + P_2)}$; this by sine of inclination gives the perpendicular height of a, and by cosine gives the horizontal distance from the foot of the perpendicular to P_1P_2.

To compute the distance P_1P_2 and the bearing of this line, Denning depends on topographical maps, while Newton uses the method of middle latitude sailing. The following method may also be applied, which assumes a spherical earth, and avoids the inconveniences due to changes of scale, etc., on ordinary maps.

In figure C, N is the north pole of the earth, P_1 has geographical position ϕ_1,l_1, P_2 has position ϕ_2,l_2, γ is the great circle arc connecting P_1 and P_2. Then

$$\sin \frac{1}{2}\gamma = \sin \frac{1}{2}(\phi_2 - \phi_1) \left[1 + \cos \phi_2 \cos \phi_1 \frac{\sin^2 \frac{1}{2}(l_2 - l_1)}{\sin^2 \frac{1}{2}(\phi_2 - \phi_1)} \right]^{\frac{1}{2}}.$$

In this, whole angles may be substituted for the sines of half angles, for three place or slide rule work to 9° 3′, or for four place work to 3° 43′. Then

$$\gamma = (\phi_2 - \phi_1) \left[1 + \cos \phi_2 \cos \phi_1 \left(\frac{l_2 - l_1}{\phi_2 - \phi_1} \right)^2 \right]^{\frac{1}{2}}$$

which is extremely convenient for slide rule work. For meteor paths short enough to be regarded as straight (which includes all but the very long paths of some large fireballs) this equation is amply accurate. Within these limits also the chord P_1P_2 equals the arc P_1P_2, with sufficient accuracy.

The spherical angles at P_1 and P_2 may be found by the sine rule, when not too near 90°. Otherwise, by use of the bisected isosceles triangle P_2NQ,

$$\cot NP_2Q = \sin \phi_2 \tan \frac{1}{2}(l_2 - l_1),\ P_1QP_2 = 180^\circ - NP_2Q,$$

$$\sin QP_2P_1 = \sin (\phi_2 - \phi_1) \sin P_1QP_2/\sin \gamma,$$

whence P_2; and similarly for P_1. For small angles these equations are convenient for slide rule work, simplifying to

$$NP_2Q - 90^\circ = \frac{1}{2}(l_2 - l_1) \sin \phi_2,$$

$$\sin QP_2P_1 = \sin NP_2Q \cdot (\phi_2 - \phi_1)/\gamma, \quad = (\phi_2 - \phi_1)/\gamma \text{ usually.}$$

The mean of the bearings at P_1 and P_2 is used for the bearing of P_1P_2 and in locating P_1' and P_2' on the horizon of the oriented globe.

[1] H. A. Newton, *Am. J. Sci.* (2), **47**, 402 (1868).
[2] W. F. Denning, *Telescopic Work for Starlight Evenings*, 278, London (1891).

A STUDY OF METEOR LIGHT CURVES

By Dorrit Hoffleit

Harvard College Observatory, Cambridge, Massachusetts

Communicated December 23, 1932

A cursory examination of some fifty miscellaneous meteor photographs is sufficient to impress one not only with the diversity in kinds of meteor trails but more particularly with the definite resemblances which exist between several of the trails. In order to investigate the details of this similarity the present survey of the relative changes in brightness along the entire photographed path of certain meteors was undertaken. The data are here presented together with a comparison of the trails studied.

At first about twenty of the most uniform trails were selected from plates of the different series, and the density at regular intervals along a trail was compared with a photographic wedge. The wedge, with a linear scale photographed simultaneously beside it (made for the purpose by the late Prof. King), was adjusted in the focal plane of an eyepiece of a compound microscope, so that optical contact between the meteor trail and the plane of the wedge was secured. In estimating densities only the arbitrary scale readings of the wedge were recorded, and no attempt was made to give ranges in terms of the magnitudes of star images on the various plates.

The results obtained from the sample selection of plates seemed to indicate that further investigation might prove of interest, but it was decided

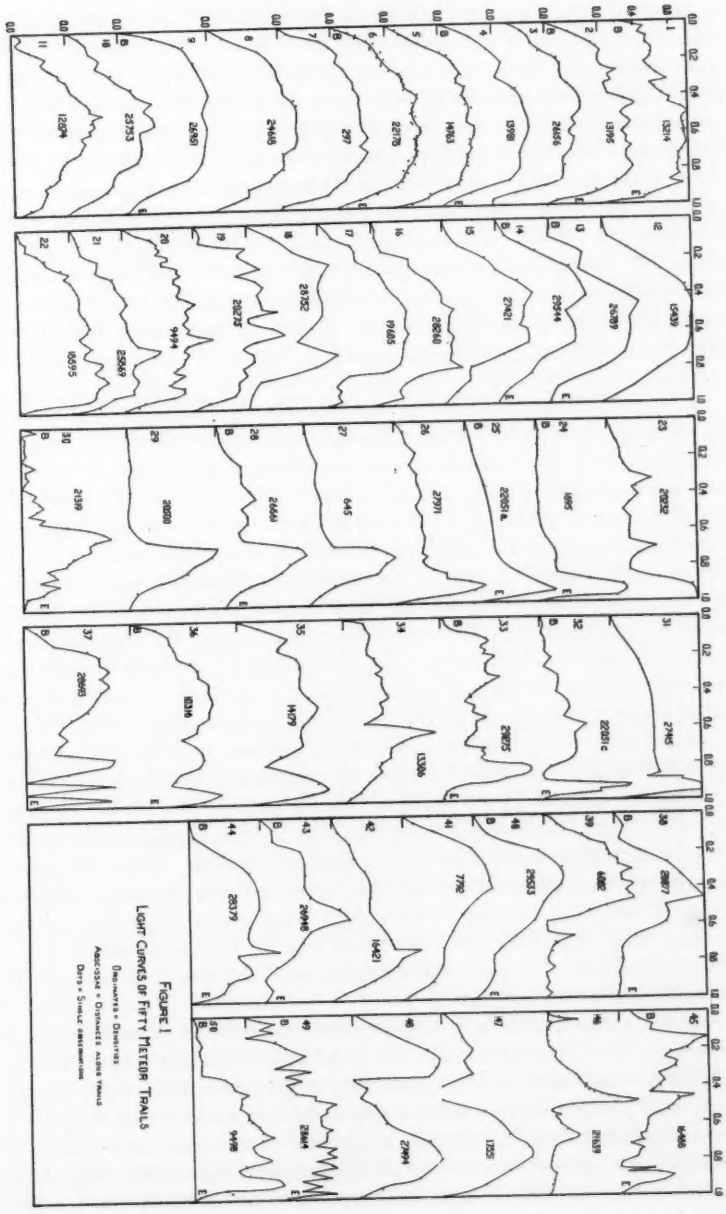
FIGURE 1
LIGHT CURVES OF FIFTY METEOR TRAILS
ORDINATES = DENSITIES
ABSCISSAS = DISTANCES ALONG TRAILS
DOTS = SINGLE OBSERVATIONS

to limit the first discussion to a single plate series. The *AI* series (made with three different lenses as described in *Harvard Annals*, **87**, 233, 1931) was chosen partly because it contains the largest number of meteor photographs, but mainly because many of the trails are so short that a difference in the scale of the plate between the beginning and the end of a trail is not important. All the meteor photographs of the series were examined: those trails which ran to the edges of the plates (about fifteen per cent) were rejected, and of the others the fifty least complicated were selected, representing about half of the total available trails not limited by the field of the plates. It did not seem worth while to study the complex trails in detail, for a rapid examination revealed similarity of trails only among those in which the variation was comparatively simple. Furthermore, the method used for estimating changes in density is unsuitable for rapid complex variations.

To emphasize the fact that the variations in light along several meteor paths have something in common, the light curves were plotted on bases of the same size. The resulting curves are arranged arbitrarily in figure 1. Two principal types (designated Type I and Type II) seem to be apparent. The first is characterized by a fairly smooth curve with a broad maximum, sometimes symmetrical, but generally with a steeper descending branch (Fig. 1, first column). Type II curves represent the frequently observed hair-line spindle trails, which, as the term implies, are due to meteors which are faintly visible a large fraction of their entire paths, then brighten suddenly and vanish nearly as rapidly. Both classes have been subdivided. For Type I there are two principal groups. To the first, I*a*, belong curves 1–7 in figure 1; and to the second group, I*b*, belong curves 12–15. Type I*b* differs from I*a* by having maximum brightness more central and the curve less broad. Curves 16 and 17 are similar and also form a subclass of Type I. Curves 18–22 are less regular examples of Type I. The curves of Type II have been divided into three groups, though they actually form a continuous sequence rather than distinct groups. When the maximum occurs beyond 0.8 of the distance between the initial and vanishing points of the trail, the curves have been assigned to Type II*a* (curves 23–26); when maximum is between 0.65 and 0.8 the curves are of Type II*b* (curves 27–29); and for maximum between 0.5 and 0.65 they are of Type II*c* (curves 30 and 34).

Figure 2 shows similar curves superposed, and the groups arranged in a sequence. It will be noted that for Type II the relative lengths of the spindles are correlated with the positions of maximum brightness, a relatively long spindle corresponding to an early maximum. This may be a spurious result due to the limiting magnitude of the plate, since many of the hair-lines are not of constant, but of slightly increasing brightness, and the curves are plotted on proportional parts of the trail; nor is it im-

possible that short trails assigned to Type I are really only spindles of what would have been classed as curves of Type II if the plates had been capable of recording fainter images.

Table 1 is arranged according to the numbers of the *AI* plates and gives in successive columns the corresponding numbers of the light curves represented in figure 1, the date, the lengths in centimeters and degrees, the

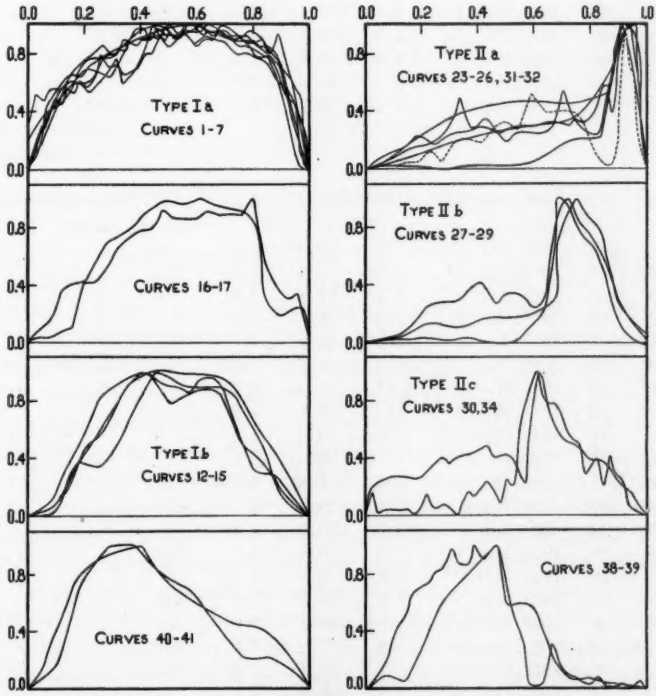

FIGURE 2

Similar light curves from figure 1, superposed (coördinates the same).

maximum density in terms of the wedge (where 0 represents clear film, and 5.5 represents maximum possible density) and the type of curve.

In table 2 are listed the lengths of curves of Types I*a*, I*b*, II*a*, II*b* and II*c*, and the average length for each of these types. The average length for all Type II curves is 8°.0 with a spread from 1°.0 to 19°.1; only three curves are longer than ten degrees. The average length for Type I*a* is 16°.6 with a range from 11°.0 to 26°.3, and no trail shorter than ten degrees. It is apparent that the spindles alone of Type II are shorter than

TABLE 1

SELECTED METEOR PHOTOGRAPHS

PLATE	CURVE (FIG. 1)	DATE	LENGTH CM.	LENGTH °	WEDGE MAX.	TYPE	NOTES
297	7	1902, Sept. 2	6.4	21.2	3.25	Ia	Measured principal component only
645	27	1903, Jan. 18	1.3	3.4	3.2	IIb	
1695	24	1903, Nov. 20	2.2	4.95	5.2	IIa	
6082	39	1907, Aug. 28	5.9	10.6	2.3		
7792	41	1909, May 11	1.2	...	4.5		
9494	20	1910, Dec. 12	6.0	17.9	2.9	I	
9498	50	1910, Dec. 12	1.9	6.4	1.8		
10316	36	1911, Nov. 16	3.0	10.5	3.8		
12874	11	1914, Sept. 17	5.4	17.8	5.5	I	Spindle at center manifested chiefly by widening of trail
13195	2	1914, Dec. 10	4.4	14.2	3.85:	Ia	Trail widens at maximum
13214	1	1914, Dec. 12	3.8	13.6	3.85	Ia	
13306	34	1914, Dec. 26	4.25	13.6	2.5	IIc	
13981	4	1915, Aug. 14	4.2	14.3	4.0:	Ia	
14179	35	1915, Oct. 24	2.0	5.75	1.5		
14763	5	1916, Apr. 6	4.9	15.9	3.7	Ia	
15439	12	1916, Dec. 10	0.5	1.8	2.05	Ib	A spindle
16421	42	1917, Nov. 2	1.4	5.05	4.25		
16488	45	1917, Nov. 11	1.2	6.1	3.5		
17551	47	1918, Sept. 15	1.9	6.0	4.0		
18595	22	1919, June 12	4.1	12.0	2.9	I	
19605	17	1920, Mar. 24	3.9	8.8	3.35	I	
20232	23	1921, Jan. 6	2.9	9.9	3.5	IIa	
20275	19	1921, Jan. 17	2.7	10.5	1.85	I	
20500	29	1921, Mar. 4	1.7	5.6	2.7	IIb	
20877	38	1921, July 31	0.8	2.8	3.5		
21319	30	1921, Nov. 5	5.6	16.8	3.0	IIc	
21639	46	1922, Feb. 25	8.6	28.6	3.0		
22051a	25	1922, Oct. 20	0.3	1.0	3.2	IIa	
22051c	32	1922, Oct. 20	2.7	7.7	3.0	IIa	
22178	6	1922, Dec. 12	7.8	26.3	3.9	Ia	
24618	8	1926, Mar. 6	11.8	39.1	3.0	I	Measured principal component only; both ends in region of poor definition
25753	10	1927, Sept. 27	7.3	23.7	3.9	I	The brighter component; one end in region of poor definition
25869	21	1927, Oct. 26	1.1	3.6	3.2	I	
26156	3	1928, Jan. 30	3.15	11.0	2.55	Ia	
26561	28	1928, Aug. 11	1.2	4.2	3.7	IIb	
26789	13	1928, Nov. 15	2.3	6.9	1.35	Ib	A spindle

PLATE	CURVE (FIG. 1)	DATE	LENGTH CM.	LENGTH °	WEDGE MAX.	TYPE	NOTES
26948	43	1929, Jan. 2	3.2	10.6	1.8		
26951	9	1929, Jan. 2	1.2	4.7	2.15	I	
27415	31	1929, July 31	0.8	2.2	3.8	IIa	
27421	15	1929, Aug. 2	1.8	7.0	2.1	Ib	
27494	48	1929, Aug. 26	1.0	2.75	2.65		
27971	26	1930, Feb. 24	5.8	19.1	3.4	IIa	
28260	16	1930, June 25	2.7	7.5:	2.65	I	
28379	44	1930, Aug. 10	0.9	4.6	2.15		
28614	49	1930, Oct. 21	5.2	17.1	2.0		
28693	37	1930, Nov. 22	3.0:	9.8	2.1		
28752	18	1930, Dec. 16	0.8	2.5	1.2	I	
29275	33	1931, Aug. 5	5.8:	17:	2.0	IIa?	
29533	40	1931, Nov. 9	1.3	4.0	0.95		
29544	14	1931, Nov. 11	1.3	4.6	1.15	Ib	

half the entire photographed paths; it therefore seems probable that Types I*a* and II are really distinct. For Type I*b* curves, however, the average length is 5°.1 with a range from 1°.8 to 7°.0, so that the latter may be incompletely photographed Type II curves. Curve 45 from plate AI16488, though not a Type I curve, is of interest in this connection. The same meteor was photographed on AC19444, a much longer path being recorded. The *AC* plate shows a long hair-line, much fainter than the portion of the path photographed with the *AI* camera, which recorded only a fraction of the spindle. The *AC* plate is overexposed for the maximum, however, so that the interesting detail of three sharp secondary spindles is practically lost, and is evidenced only in a widening of the trail, not by increased density. Similarly, details of many trails are lost by overexposure. Where only wedge comparisons are made the curves may be flat at maximum (the maximum density of which the plate is capable). The difficulty might be partially overcome by adding corrections for increased width; this has not been done for the first approximations, but for the curves that are likely to have been affected by plate limitations notes are given in table 1.

A different kind of observation (*Pop. Ast.*, **39,** 606, 1931) also seems to

TABLE 2

LENGTH OF CURVES OF DIFFERENT TYPES

TYPE I*a*		TYPE I*b*		TYPE II*a*		TYPE II*b*		TYPE II*c*	
Curve	Length	Curve	Length	Curve	Length	Curve	Length	Curve	Length
1	13°.6	12	1°.8	23	9°.9	27	3°.4	30	16°.8
2	14.2	13	6.9	24	4.95	28	4.2	34	13.6
3	11.0	14	4.6	25	1.0	29	5.6		
4	14.3	15	7.0	26	19.1			Mean	15°.2
5	15.9			31	2.2	Mean	4°.4		
6	26.3	Mean	5°.1	32	7.7				
7	21.2								
				Mean	7°.4				
Mean	16°.6								

emphasize the question whether photographic or optical limitations alone can account for the observation of two types of curves instead of one. Two Texas variable star observers saw almost simultaneously a telescopic and a naked eye meteor, respectively. The visual meteor appeared over twenty degrees from the field of the telescope, but the plotted paths when projected were separated only by the probable error of observation. Did the light of the meteor increase gradually and uniformly (as for Type I*a*), or was it very faint most of the twenty degrees, then brightened suddenly?

It was hoped that these types might be correlated with other known facts about meteors. The data given in the Meteor Catalogue (*H. A.*, **87**, 233ff, 1931) were examined but yielded nothing of interest. If any correlations do exist, they should involve heights and velocities. Individual heights could not be determined. For the purpose of getting velocities the trails were examined for their possible association with known radiants by plotting the paths together with radiant points on an eighteen inch Johnston celestial globe. Only those radiants given in the Observer's Handbook (R. A. S. of Canada, 1932) were used, and among them the Scorpiids, Sagittids and Arietids were rejected as unreliable. No radiant was assigned to a trail that did not occur within ten days of the maximum of the shower. Of the fifty trails, twenty-one appeared to come from well determined radiants, namely, five Geminids, four Leonids, four Perseids, three Orionids, two Taurids, two Quadrantids and one δ Aquarid. For these trails the letters *B* and *E* on the curves of figure 1 indicate which are the initial and which the vanishing points. It is possible that where radiants could not be assigned the curves are incorrectly oriented; and sometimes assigned radiants are erroneous if the meteor was headed toward instead of away from the radiant.

Geocentric velocities, assuming parabolic orbits, were computed using an eighteen inch globe and a ten inch slide rule (Olivier, *Meteors*, p. 172, 1925) but were not corrected for zenith attraction.

Except for two of the Leonid trails which seem to be spindles only, larger velocities correspond on the whole to Type II trails than to Type I, but the number of observations was too small to warrant definite conclusions; hence all the trails listed in the Meteor Catalogue were examined for radiants. For those that did appear to come from well determined radiants, the fraction of the trail at which maximum brightness occurred was recorded and the velocity computed. A total of sixty-seven trails apparently associated with shower radiants were found. For the data see table 3; the velocities are given to the nearest half kilometer a second.

Disregarding the Leonids that do not have Type II trails, and one Geminid, there appears to be a correlation between the position of maximum light and velocity, though with considerable scattering (see Fig. 3). The scattering does not seem excessive, however, when one considers the

many sources which may contribute to it for any given shower, important among which are plate differences, differences in atmospheric conditions, in the angles at which the meteors strike the atmosphere and differences in mass, size and shape of the meteors. Hence the correlation is not thought to be entirely accidental.

Two sources may account for the very large scattering in the case of the Leonids which are the fastest meteors represented. For some of the points to the left of the general sequence of points, the limiting magnitude of the plate may be responsible, by having failed to record the hair-line. For some meteors that occurred near the radiant another explanation seems plausible. Leonids have been observed to leave streaks which are fairly bright and which persist for several seconds after the meteors themselves have disappeared; also fireballs have been seen to leave trains lasting as long as twenty minutes (Olivier, *Meteors*, p. 23, 1925). When the path

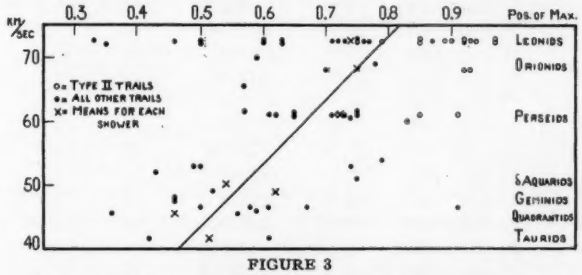

FIGURE 3

Positions of maximum density on meteor trails plotted against geocentric velocities.

of a meteor crosses the line of sight of the camera, such a streak or train would probably not alter the relative intensity of the hair-line and of the spindle appreciably; but when the direction of the meteor is at a small angle to the line of sight so that the apparent path is very short, a sensibly bright stationary train might cause a spurious shift of maximum light toward the initial point. Hence the mean of the Type II Leonids alone may be more nearly the true mean position of maximum light for that swarm. Except for the three trails AI26789, AI29533 and E6701a, the Leonids to the left of 0.7 in figure 3 are shorter than 1°.25.

The one Geminid (AI9498, curve 50, Fig. 1) which does not lie in the general sequence, but well to the right of it, brings us again to the question of the cause of the absence of hair-lines. It may be remarked that if the final spindle of this particular trail is disregarded, and the maximum considered at 0.66 (the maximum of the broad curve on which the spindles are superposed), then this curve would follow the general sequence of figure 3.

Table 4 gives the mean velocity and mean position of maximum bright-

TABLE 3

PHOTOGRAPHS OF METEORS BELONGING TO SHOWER RADIANTS

SHOWER	DATE	VEL. KM./SEC.	PLATE	POS. OF MAX.	LENGTH °	TYPE
Quadrantids	2 Jan. 1929	45.5	AI26948	.56	10.6	
	2 Jan. 1929	45.5	26951	.36+	4.7	I
δ Aquarids	25 July 1903	52.0	B32329	.43	2.3	
	26 July 1905	51.0	AM3741	.75	1.5	I
	29 July 1913	49.0	AC14225	.52+	3.4	
	31 July 1921	48.5	AI20877	.46	2.8	
Perseids	5 Aug. 1931	60.0	AI29275	.83	...	II
	6 Aug. 1912	60.5	11014	.74	5.7	
	8 Aug. 1923	61.0	22643	.65	15.0	
	8 Aug. 1899	61.0	AC387	.61:	12.2	I
	9 Aug. 1927	61.0	AY1553	.62	19.1	I
	10 Aug. 1930	61.0	AI28379	.73	...	
	10 Aug. 1900	61.0	AC958	.91	3.2	II
	10 Aug. 1900	61.0	959	.85	2.0	II
	11 Aug. 1910	61.0	AC11847	.65	6.6	I
	11 Aug. 1925	61.0	AY738	.71	0.9	
	11 Aug. 1928	61.0	AI26561	.72	4.2	II
	12 Aug. 1925	61.0	AY740	.75	0.3	
	13 Aug. 1906	61.5	AC7700	.75	4.6	I
	14 Aug. 1915	61.5	AI13981	.57	14.3	I
Orionids	14 Oct. 1931	70.0	MF16144	.59	1.6	
	17 Oct. 1924	69.0	AY316	.78	5.7	I:
	20 Oct. 1922	68.0	AI22051a	.93	1.0	II
	20 Oct. 1922	68.0	22051c	.92	7.7	II
	21 Oct. 1930	68.0	28614	.7:	17.1	
	26 Oct. 1901	65.5	AC1913	.57	5.0	I
Taurids	11 Nov. 1917	41.5	AC19444	.61	10.7	
	11 Nov. 1931	41.5	AI29544	.42	4.6	I
Leonids	9 Nov. 1931	72.0	AI29533	.35	4.0	
	13 Nov. 1897	72.5	E3681	.63	0.8	I
	14 Nov. 1898	72.5	E4578b	.89	6.8	II
			4581	.63	1.2	I
			4582	.50:	0.4	I
			4594	.97	14.4	II
			4601a	.92	7.2	II
			4601b	.6:	0.6	I
			4611b	.6:	0.6	I:
			4617	.79	2.4	II
			4623b	.77	1.6	I
			4624	.75	2.5	Peculiar
			4625	.5:	0.8	I
			4630	.97	15.7	II
			4637a	.85	2.1	II
			4638a	.75	2.55	II:
			4638b	.72	1.7	I
			4650	.94	5.8	II
			4656a	.71	8.2	

SHOWER	DATE	VEL. KM./SEC.	PLATE	POS. OF MAX.	LENGTH °	TYPE
	14 Nov. 1901	72.5	6701a	.33	2.5	Spindle
			6701b	.87	2.4	
			6701c	.90	4.7	II
	14 Nov. 1904	72.5	AC5530	.76	2.0	I
	15 Nov. 1901	72.5	E6726	.85	2.55	II
	15 Nov. 1928	72.5	AI26789	.46	6.9	I
	16 Nov. 1900	72.5	E6310:	.73	5.6	I
	16 Nov. 1911	72.5	AI10316	.94	10.5	
	20 Nov. 1903	72.5	AI1695	.93	4.95	II
Geminids	1 Dec. 1908	54.0	AI7264	.79	5.5	
	2 Dec. 1899	53.0	AC561a	.49	6.0	
	2 Dec. 1904	53.0	5653	.50	2.2	I
	4 Dec. 1931	52.0	B55641	.74	5.3	
	10 Dec. 1914	48.0	AI13195	.46+	14.2	I
	12 Dec. 1910	46.5	9494	.61:	17.9	I
	12 Dec. 1910	46.5	9498	.91	6.4	
	12 Dec. 1914	46.5	13213	.67	15.3	
	12 Dec. 1914	46.5	13214	.5	13.6	I
	12 Dec. 1922	46.5	22178	.58	26.3	I
	13 Dec. 1926	46.0	AX1999	.59	21.6	

ness for each of the radiants represented, except that, for the Leonids the total mean and the mean of Type II trails only are recorded, and for the Geminids the mean of the observations both with and without AI9498. The third column gives the number of trails represented. The first two columns are plotted with crosses in figure 3.

TABLE 4

MEAN VELOCITY AND MEAN POSITION OF MAXIMUM BRIGHTNESS

RADIANT	VEL. KM./SEC.	POS. OF MAX.	NO. PTS.
Quadrantids	45.5	0.46	2
δ Aquarids	50.1	0.54	4
Perseids	61.0	0.72	14
Orionids	68.1	0.75	6
Taurids	41.5	0.51	2
All Leonids	72.5	0.74	28
Leonids II	72.5	0.89	11
All Geminids	49.0	0.62	11
Geminids except AI9498	49.2	0.59	10

To summarize the investigation: It is found (1) that the simple meteor trails fall into two principal groups, those with and those without initial hair-lines; (2) a statistical relation exists between the fraction of the photographed path at which maximum brightness occurs and the velocity at which the meteor strikes the earth's atmosphere, namely, the greater the velocity, the nearer to the vanishing point does the meteor become brightest.

I am indebted to Dr. W. J. Fisher for many helpful suggestions and discussions during the progress of this investigation.

ABSORPTION AND SPACE REDDENING IN THE GALAXY AS SHOWN BY THE COLORS OF GLOBULAR CLUSTERS

By Joel Stebbins

Mount Wilson Observatory, Carnegie Institution of Washington

Read before the Academy, November 14, 1932

The globular clusters, because of their great distances and intrinsic luminosities as compared with individual stars, furnish an excellent means for testing the transparency of space in the neighborhood of our galactic system. The photoelectric cell, when applied to the photometry of such objects, has the advantage of integrating the light effect from a luminous surface or a group of stars, and thus the total light or color of a cluster may be compared with that of a standard star. The present report is based upon observations made at Mount Wilson during the past year with a photoelectric cell attached to the 100-inch reflector. The photometer used was that which has been in operation for a number of years at the Washburn Observatory. The gas-filled potassium hydride cell by Kunz is of the type we have applied to the photometry of stars, and its construction in a quartz bulb eliminates the dark current, which is troublesome when currents of 10^{-14} or 10^{-15} amperes are to be measured. The rate-of-charge method with a Lindemann electrometer was used throughout the investigation.

For measures of color the instrument is furnished with filters, which may be conveniently interposed in front of the cell. With a cell having a maximum sensitivity at 4500 Å, the blue and yellow filters give effective maxima at about 4300 Å and 4800 Å, respectively. Between stars of spectrum A0 and K0 the combination gives a difference in color-index of 0.44 mag. This amount is not a large leverage for the determination of color-indices, but it maintains the possibility of reaching faint objects. At the Newtonian focus of the 100-inch reflector the ordinary limit for satisfactory measures of the total light of a star, nebula or cluster is about photographic magnitude 13.0, and with the loss in the filters the limit for colors is about 12.5. These limits can be extended somewhat, but for fainter objects the elimination of the effect of the sky background becomes increasingly difficult. The faintest object actually observed for total light was of magnitude 14.6, and satisfactory color-indices have been found for clusters and nebula ranging from 12.5 to 13.0. Since the recognized globular clusters are brighter than the thirteenth magnitude, it is possible to observe all of them that can be reached from Mount Wilson, that is, all those north of declination $-30°$.

The procedure of observation was always to measure a star of known magnitude and spectrum near each cluster, for a check upon the atmos-

pheric extinction, for calibration of the color scale and for reference to a system of magnitudes. Usually the comparison stars were taken from the Draper Catalogue, and the objects selected were those for which precise Harvard visual magnitudes are available. The calibration of color-index against spectral type depends, however, upon the Mount Wilson system for giant stars, and the scale, based upon 133 stars measured photoelectrically at Mount Wilson and Madison, is as follows:

SPECTRUM	COLOR-INDEX	SPECTRUM	COLOR-INDEX
B5	−0.36 mag.	G0	−0.06 mag.
A0	−0.30	G5	+0.03
A5	−0.24	K0	+0.14
F0	−0.19	K5	+0.25
F5	−0.13		

The observations were made on fourteen nights extending from September, 1931, to July, 1932, most of them during the last two months of the interval. The results in the table are for 47 objects, just about half the globular clusters known to be immediately related to our own galaxy. The details of the measures are left for a further publication. The galactic latitude is referred to Newcomb's pole at right ascension $12^h\ 44^m.4$, declination $+26°.8$ (1900). The number of observations is uniformly the number of nights on which the object in question was measured.

The tabulated results are also shown in figure 1, where each cluster with reduced weight is indicated by a cross. The reddening in low galactic latitudes is obvious. It would be better to discuss the color-excesses of the clusters in relation to their respective spectral types, but for most of the objects the equivalent spectra are not available.

On the assumption that a thin homogeneous absorbing layer near the plane of the galaxy produces the differential color effect, the calculated color-index of a cluster C, in magnitudes, is found by a least-squares solution from 42 equations to be

$$C = \underset{\pm 14}{-0.081} + \underset{\pm 18}{0.0237}\ \csc b, \qquad (1)$$

where b is the galactic latitude (taken without regard to sign) and the term −0.081 mag. is the mean unobscured color-index of the clusters, corresponding to spectral class F8. The probable error of one color-index is ±0.055 mag., or about 0.3 of a spectral class. The residual for a cluster includes the error of observation, the deviation from average color and the effect of any irregularity in the space absorption.

The solution is quite sensitive to the choice of the galactic plane, and Newcomb's pole was selected in order to use the convenient Tables of Galactic Coördinates by P. Emanuelli.[1] The Harvard system with pole at $12^h\ 40^m$, $+28°$ (1900) has the disadvantage that it places one cluster,

COLOR-INDICES OF GLOBULAR CLUSTERS

N. G. C.	GALACTIC LATITUDE	COLOR-INDEX Mag.	NO. OBS.	N. G. C.	GALACTIC LATITUDE	COLOR-INDEX Mag.	NO. OBS.
2419	+25°	−0.17	1	6517[3,4]	+ 6°.5	+0.44	2
4147	+78	−0.07	1	6522	− 3.9	+0.13	1
5024	+80	−0.09	1	6528	− 4.1	+0.20	1
5053[1]	+79	(−0.39)	1	6535[3]	+10	0.00	2
5466	+73	−0.05	2	6539[3,4]	+ 6.5	+0.33	2
5634	+50	−0.03	1	6553	− 3.1	+0.39	2
5904	+47	−0.04	1	6569	− 6.6	+0.13	1
6121	+16	+0.08	1	6626	− 5.6	+0.09	2
6144	+16	+0.02	2	6637	−10	+0.08	1
6218	+26	+0.01	1	6638	− 7.2	+0.06	2
6254	+23	+0.03	1	6656	− 7.6	+0.04	1
6293	+ 7.9	+0.02	2	6712	− 4.7	+0.07	1
6304	+ 5.5	+0.21	1	6760	− 4.4	+0.40	2
6316	+ 5.9	+0.21	1	6779	+ 7.5	−0.04	2
6325	+ 8.1	+0.27	1	6809	−23	−0.09	1
6333	+11	+0.08	1	6864	−26	+0.01	3
6342	+ 9.7	+0.18	1	6934	−20	−0.04	2
6356	+10	+0.11	1	6981	−33	−0.04	1
6366[2]	+16	+0.32	2	7006	−20	−0.07	4
6402	+14	+0.12	2	7078	−28	−0.08	3
6426[3]	+16	−0.06	2	7089	−37	−0.06	3
6440	+ 3.7	+0.31	3	7099	−47	−0.11	2
6441	− 4.8	+0.18	1	7492[2]	−64	−0.21	2
6453	− 3.8	+0.21	1				

[1] Probably not a globular cluster.
[2] Omitted.
[3] Weight 0.5, faint.
[4] Measures discordant.

N. G. C. 6440, in latitude +2°.3, and if included in the solution, this object receives excessive weight. There seems to be no reason why the plane of the absorbing material should be coincident with the galactic plane determined from limited groups of stars, and the precise determination of this plane is left until further data have been obtained.

In figure 1 it may be noted that the clusters show a preponderance of negative residuals in south latitude and of positive residuals in north latitude. This result may be due partly to the choice of the galactic plane and partly to the sun's position in space. Making a solution similar to (1), but with different values of the absorption north and south, we find:

$$\begin{aligned} C &= -0.096 \pm 13 + 0.0312 \pm 24 \csc b \quad \text{(North)} \\ C &= -0.096 \pm 16 + 0.0223 \csc b \quad \text{(South)} \end{aligned} \tag{2}$$

No significance at present is assigned to the difference between the two

sides of the galaxy, but the sum of the two coefficients, 0.0312 + 0.0223 = 0.0535 mag., gives the total photoelectric differential absorption by the assumed layer in a direction normal to the galactic plane. The factor for reduction to Seares's[2] system is the ratio of the two scales for color-index, 1.48/0.44 = 3.36, which gives 0.180 mag. for the photograph *minus* the visual absorption. For the space absorption per thousand parsecs P. van de Kamp[3] found the values, photographic 0.67, visual 0.34, or a differential of 0.33 mag.; and combining this difference with the present determination, we find for the equivalent thickness of the absorbing layer,

$$h = 540 \pm 60 \text{ parsecs.}$$

This result is about twice the thickness of the absorbing layer derived by

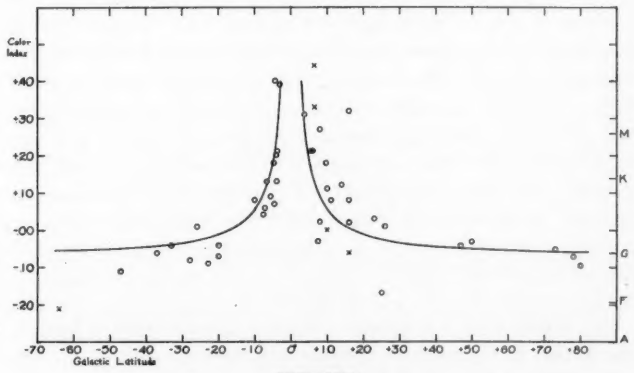

FIGURE 1

Color-indices of globular clusters.

R. J. Trumpler[4] in a study of open clusters, namely, 200–300 parsecs, and about three times the 175 parsecs found by van de Kamp from a variety of evidence. The globular clusters are probably sufficiently remote to show practically all the absorption there is in the galactic system.

We now proceed to apply these results to a correction of Shapley's distances of globular clusters, which were derived on the assumption of transparent space. For a given cluster the photoelectric differential absorption in magnitudes is assumed from (1) to be 0.0237 csc b. The correcting distance factor f is given by the relation,

$$\log f = -0.0237 \cdot \frac{1.48}{0.44} \cdot \frac{0.67}{0.33} \cdot \frac{0.4}{2} \csc b \cdot \qquad (3)$$

$$= -0.0324 \csc b$$

The value of f varies from 0.25 for 3°.1, the lowest latitude of a cluster, up to 0.93 at the pole. Figure 2 shows (*a*) Shapley's[5] system of globular clusters projected on the XZ-plane and (*b*) the system after the distances have been corrected by the proper factors. The first feature to be noticed in the revised system is the reduced extension in the equatorial direction. Instead of several clusters out at 50,000 parsecs, there are only one or two at projected distances of more than 30,000 parsecs from the sun. The region of avoidance, which presumably is simply the space where no clusters can be seen because of the absorbing layer, is reduced in thickness from 2500 to 1100 parsecs. The center of the system, which Shapley placed at 16,000 parsecs, is now found at 10,000 parsecs from the sun. The general form of the system appears somewhat more reasonable, being more nearly symmetrical and also more condensed about the center.

It will be noted that the clusters just below or south of the galactic plane

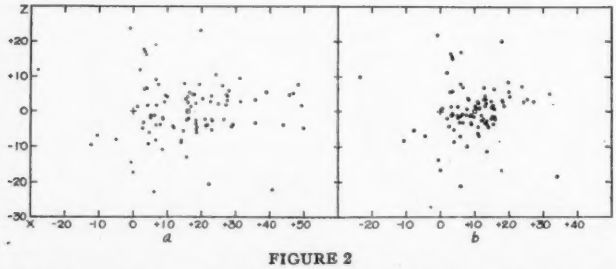

FIGURE 2

The general system of globular clusters projected on the XZ-plane, coördinates in thousands of parsecs: (*a*) Shapley's system; (*b*) the same revised on the basis of absorption.

have been drawn in more toward the sun than those to the north. This indicates that probably the correction factors, which correspond to the negative residuals in figure 1, are relatively too large on the south side. This difference in the system between south and north may be reduced somewhat by applying separate corrections computed from (2), but as a first approximation it is sufficient to treat the absorbing layer as symmetrical with respect to the adopted galactic plane.

The relatively large size of our own galaxy has long been an obstacle in considering it as a system quite similar to the extra-galactic nebulae, but this difficulty is to a great extent diminished when the inferred dimensions of the galaxy are corrected for absorption. In a comparison of the galactic system with, for instance, the Andromeda Nebula we must adopt the same basis in each case. Hubble[6] has found over a hundred objects in the Andromeda Nebula, tentatively identified as globular clusters, some of which

are far outside the limits set by the star clouds of the nebula. Until the search for such clusters in Andromeda is completed it is premature to compare that system with the general group of globular clusters associated with the galaxy. We therefore consider the obvious extent of the nebula to be as shown on photographs, to which Hubble assigns an apparent diameter of 160′. At a distance of 250,000 parsecs this value corresponds to a linear diameter of 12,000 parsecs, which, corrected for absorption with the factor $f = 0.83$ for latitude 23°, becomes 10,000 parsecs.

The possible effect of absorption upon the inferred dimensions and characteristics of the galaxy, and the close analogy of our system with the Andromeda and other nebulae have been discussed by Seares[7] in several papers. It is true that Trumpler, with allowance for absorption, derives a value of 10,000 parsecs for the diameter of the flattened system of open clusters, which he presupposes to outline the galaxy, but unless the evidence for galactic rotation is all wrong, his dimensions in the direction of the center of globular clusters will have to be increased. If we allow an extent of 5000 parsecs from the sun for the stars in the direction of the anti-center, and 10,000 parsecs to the center, we have a radius of 15,000 and a diameter of 30,000 parsecs for a galaxy still symmetrical and concentric with the system of the globular clusters. This result is only three times the diameter of the Andromeda Nebula and is certainly more plausible than an overall dimension of the order of 80,000 parsecs which has been inferred from the uncorrected distances of clusters. A sphere of radius 15,000 parsecs would include four-fifths of the globular clusters, and those outside may be considered as stragglers, for no one thinks that the spaces between the outer clusters are filled with stars.

It may be noted that any obstruction in space in addition to that accompanied by scattering as shown by the reddening of clusters will require a further reduction of all distances based upon photometric considerations; but if the absorption is in the galaxy and near the sun, objects in the same direction, whether galactic or extra-galactic, will be affected in the same measure. I have in hand a further study of the magnitudes and colors of some forty extra-galactic nebulae observed at Mount Wilson, and also of about 700 *B*-stars observed by C. M. Huffer and myself at Madison. It is hoped that from this material further evidence on space absorption will be secured.

The conclusions from the present study are that when allowance is made for absorption the distances of some of the clusters in low latitude are only one-fourth as great as have sometimes been supposed; that the diameter of the galactic system of stars is reduced from 80,000 to possibly 30,000 parsecs; and that the great difference in size between our own galaxy and other such systems largely disappears.

[1] *Pubbl. Specola Astr. Vaticana, Rome*, **14**, 1929 (Append. 1).

[2] *Mt. Wilson Contr.*, No. 226, p. 34; *Astrophys. Jour., Chicago, Ill.*, **55** (165–237), p. 198 (1922).

[3] *Astr. Jour., Albany, N. Y.*, **40** (145–159), p. 154 (1930).

[4] *Lick Obs. Bull., Berkeley, Calif.*, **14** (154–188), p. 166 (1930).

[5] *Star Clusters*, New York, p. 175 (1930).

[6] *Mt. Wilson Contr.*, No. 452; *Astrophys. Jour., Chicago, Ill.*, **76** (44–69) (1932).

[7] *Mt. Wilson Contr.*, No. 347, p. 50; No. 428; *Astrophys. Jour.*, **67** (123–178), p. 172 (1928); **74**, (91–100) (1931); *Publ. Astr. Soc. Pacific, San Francisco, Calif.*, **43** (371–376) (1931).

AVAILABLE FOOD, RELATIVE GROWTH AND DURATION OF LIFE IN SEEDLINGS OF CUCUMIS MELO[1]

BY SOPHIA A. GOULD, RAYMOND PEARL, THOMAS I. EDWARDS AND JOHN R. MINER

DEPARTMENT OF BIOLOGY, SCHOOL OF HYGIENE AND PUBLIC HEALTH, JOHNS HOPKINS UNIVERSITY

Communicated January 4, 1933

I.—In continuation of previous work [2,3,4] from this laboratory on the growth of seedlings of the canteloup (*Cucumis melo*) grown under rigorously controlled environmental conditions, so managed that the growing plant can obtain energy and matter (other than water and air) only from endogenous sources for the purpose of metabolism, we have lately completed a study of the performance of seedlings grown from seeds from which definite portions of the cotyledons have been removed surgically prior to planting. It is the purpose of the present note to report in a preliminary way the results of these experiments, the details of which are in press elsewhere.

The cultural methods used in these experiments were identical with those used in other previously reported experiments carried out in this laboratory with the same material.[2,3,4] In the present series of experiments 145 *Cucumis melo* seeds of approximately the same weight were selected from the same melon to insure as uniform a genetic constitution as possible. The testas were removed under aseptic conditions by gentle pressure applied with forceps. The shelled seeds were then sterilized, by immersion for one minute with stirring in a 1:1000 solution of mercuric chloride, followed by rinsing in sterile, distilled water in such a way that each seed was not in contact with any other seed. Previous work has shown that this procedure followed by incubation on agar is an especially advantageous way of obtaining a uniform lot of seedlings for experimentation. Ten groups of ten seeds each were taken at random and in each group as nearly as possible the same proportion of the cotyledons was cut away with a sterile safety razor blade under aseptic precautions, and dis-

carded, care being exercised to avoid injury to the embryo. In each of the ten groups a different proportion of the cotyledons was cut away so that a series of operated seeds was available ranging from the uninjured control seeds to seeds consisting of little more than an embryo and the bases of the cotyledons. Each seed was then individually weighed and transferred, radicle downward, to an agar surface in a culture tube, for incubation in darkness at 30°C. These tubes were 60 cm. in length and 20 mm. in internal diameter, and each contained 40 cc. of a 1 per cent agar gel made up in distilled water and sterilized in an autoclave.

At 24-hour intervals the tubes were examined in a dark room, illuminated only by a photographically inactive ruby light. The height of the hypocotyl was measured in millimeters by applying a scale to the side of the glass tube. At the conclusion of the experiment each seedling was cut up into cotyledons, hypocotyl and roots, and after drying to constant weight at 98°C., the weights of each organ were recorded.

While the plan of the experiment was to have 10 seedlings in each series, this intention was not completely attained, because of accidents which one normally expects in such experimentation. The failures of the numbers in certain of the series were due to such things as imperfect germination, failure of precise geotropic response, resulting in some of the roots growing in the air and failing to penetrate the agar, failure of the hypocotyl to straighten, etc. Such abnormal seedlings were discarded, so as to leave only normal, typical specimens for the records.

Under the experimental conditions just described the growth of the seedling and its duration of life should theoretically be proportional to the amount of available food stored in its cotyledons. The primary problem of this investigation is to determine how strictly this relationship holds true. Specifically the questions asked are:

1. If a portion of the cotyledons is removed surgically, will the performance of the plant, in respect of growth and duration of life, be in all ways strictly proportional to the amount of the cotyledons left after the operation, the conditions of the experiments being such that no exogenous nourishment is available?

2. If not, what is the manner and degree of deviation from such strict proportionality?

II.—The form of the mean growth curves in each experimental series is shown in figure 1.

It is apparent from figure 1 that the growth curves in these experiments exhibit the characteristic sigmoid form of the logistic. While it is evident that the mean length of the hypocotyl is greatest in the control series, least in Series 1 with the greatest amount of cotyledonary material removed and intermediate between these two extremes in the other series in inverse

order to the amount of the cotyledons removed, it is impossible to judge visually from the diagram as to the *proportionality* between total growth of hypocotyl and available food. We may therefore turn to the consideration of table 1.

TABLE 1

RELATIVE PERFORMANCE OF NORMAL (CONTROL) SEEDS AND SEEDS FROM WHICH DIFFERENT PROPORTIONS OF THE COTYLEDONS HAVE BEEN REMOVED BY AMPUTATION. ALL FIGURES ARE PERCENTAGES OF VALUES OF THE CONTROLS TAKEN AS 100

SERIES	PER CENT OF SEED LEFT AFTER OPERATION AND PLANTED (a)	FINAL HYPOCOTYL LENGTH (b)	DRY WEIGHTS HYPOCOTYL (c)	ROOTS (d)	HYPOCOTYL PLUS ROOTS (e)	COTYLEDONS (f)	TOTAL (g)	DURATION OF GROWTH PERIOD (h)	INTERMEDIATE PERIOD (i)	TOTAL LIFE (j)
1	**10.0**	11.9	11.5	16.1	12.2	9.2	11.3	75.2	73.1	74.0
2	**14.5**	27.9	19.2	21.9	19.7	17.2	18.8	74.4	55.0	63.6
3	**19.6**	34.3	25.0	30.7	26.0	21.0	24.4	84.8	63.2	72.7
4	**24.9**	44.8	34.1	36.5	34.5	20.5	29.9	76.7	56.7	65.5
5	**31.3**	55.2	38.8	48.9	40.5	24.6	35.4	85.0	64.5	73.5
6	**40.3**	63.1	54.0	78.8	58.2	42.3	53.0	92.7	56.8	72.6
7	**49.0**	68.7	55.1	56.9	55.4	47.2	52.7	101.8	63.2	80.0
8	**59.1**	75.5	66.4	83.2	69.3	62.3	67.0	98.6	69.2	82.1
9	**76.4**	87.4	89.4	116.8	93.9	67.2	85.2	108.4	75.0	89.7
10	**90.4**	97.9	100.6	124.8	104.7	89.7	99.8	101.3	70.5	84.1
Controls	**100**	100	100	100	100	100	100	100	100	100

The plan of table 1 is to take the observed value of the controls as 100 per cent, for each variable, and then express the mean values for each experimental series derived from operated seeds, as percentages of the control values. At the beginning of the table stands a column giving relative (percentage) amount (in heavy type) of the seed left after operation in each series (mean values). These figures indicate the relative amount of food available for the seedling for growth and the continuance of life. Each subsequent column of the table is to be compared with this first one.

From the data of table 1 the following points are to be noted:

1. Excepting the dry weight of the cotyledons at the end of the experiments, no measured character of the plant upon which observations were taken exhibits relative values in the several series even remotely accordant with the proportionate amount of available nourishment in the seeds planted, as shown in the second column of table 1. This statement is true both for growth characters and for duration of life.

2. In all cases, again excepting the final dry weights of the cotyledons, the relative performance of the plant is consistently *greater* than would be expected on the basis of strict proportionality to the amount of food left in the operated seeds planted.

3. The performance of the seedlings in respect of length of hypocotyl at the end of the growth period, tends to be relatively more in excess of

expectation from the amount of food available, in those series where the larger amounts of the cotyledon had been removed surgically, with the exception only of Series 1. The differences measuring excess performance in

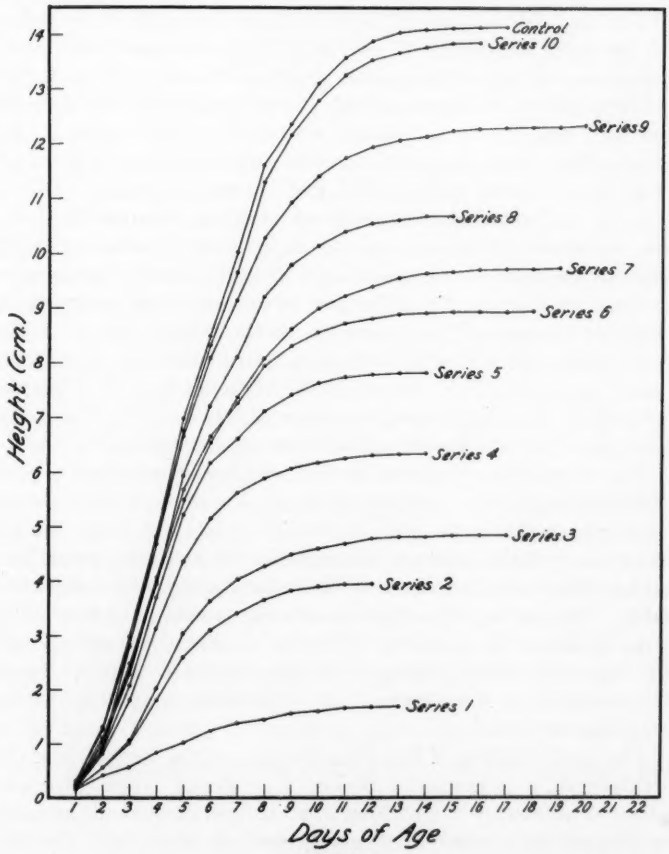
Control
Series 10
Series 9
Series 8
Series 7
Series 6
Series 5
Series 4
Series 3
Series 2
Series 1
Height (cm.)
Days of Age
0 1 2 3 4 5 6 7 8 9 10 11 12 13 14
1 2 3 4 5 6 7 8 9 10 11 12 13 14 15 16 17 18 19 20 21 22

FIGURE 1

Growth curves for the several experimental series, showing the mean length of the hypocotyl at each age. The observations are given as circles. Each curve is carried, in the diagram, only to the point where growth has ceased, i.e., where there is no further elongation of the hypocotyl.

respect of this variable (Column (b) − Column (a), table 1) are as follows: Series 1, +1.9; Series 2, +13.4; Series 3, +14.7; Series 4, +19.9; Series 5, +23.9; Series 6, +22.8; Series 7, +19.7; Series 8, +16.4; Series 9, +11.0; Series 10, +7.5.

4. The differences measuring excess performance in final dry weight of hypocotyl (Column (c) − Column (a), table 1) are: Series 1, +1.5; Series 2, +4.7; Series 3, +5.4; Series 4, +9.2; Series 4, +7.5; Series 6, +13.7; Series 7, +6.1; Series 8, +7.3; Series 9, +13.0; Series 10, +10.2.

5. The final dry weights of the roots give a quantitatively different picture from the hypocotyl. There is excess performance over expectation, but it is generally much greater in amount than in case of the hypocotyl. The differences measuring this excess performance (Column (d) − Column (a), table 1) are as follows: Series 1, +6.1; Series 2, +7.4; Series 3, +11.1; Series 4, +11.6; Series 5, +17.6; Series 6, +38.5; Series 7, +7.9; Series 8, +24.1; Series 9, +40.4; Series 10, +34.4.

6. In all the operated series without exception, the duration of the growth was greatly prolonged beyond expectation, considering the performance of the controls and the amount of food available for the growth of the operated plants. The differences measuring excess performance in this variable (Column (h) − Column (a), table 1) are: Series 1, +65.2; Series 2, +59.9; Series 3, +65.2; Series 4, +51.8; Series 5, +53.7; Series 6, +52.4; Series 7, +52.8; Series 8, +39.5; Series 9, +32.0; Series 10, +10.9. These are high values, and show plainly how great is the relative prolongation of the growth period in the operated plant.

7. The intermediate period of the life cycle, between the end of growth and the beginning of disintegration and death, also shows relative prolongation over expectation in the first eight series of operated plants inclusive. In Series 9 and 10 the intermediate period is less long than would be expected considering the performance of the controls and the amount of food available. The actual differences measuring excess (or defect) of performance (Column (i) − Column (a), table 1) are as follows: Series 1, +63.1; Series 2, +40.5; Series 3, +43.6; Series 4, +31.8; Series 5, +33.2; Series 6, +16.5; Series 7, +14.2; Series 8, +10.1; Series 9, −1.4; Series 10, −19.9.

8. The total duration of life, from planting to the beginning of death (growth period + intermediate period) is relatively prolonged over expectation, as necessarily follows from what has preceded, in all the series of plants grown from operated seeds except the last, Series 10. The differences showing amount of excess performance (Column (j) − Column (a), table 1) are: Series 1, +64.0; Series 2, +49.1; Series 3, +53.1; Series 4, +40.6; Series 5, +42.2; Series 6, +32.3; Series 7, +31.0; Series 8, +23.0; Series 9, +13.3; Series 10, −6.3.

9. The significance of the results regarding duration of life may be shown in another way. If the control seedlings had lived as long in proportion to available food as did those in Series 1 their mean total duration of life would have been slightly over 6060 hours, or 252.5 days, instead of the 816 hours, or 34 days, which they did live. In other words the life of the

seedlings in Series 1 was prolonged nearly seven and a half times more proportionately than that of the normal control seedlings. Shear[5] has reported similar prolongation of life in peanut seedlings after removal of the cotyledons.

III.—Other results discussed in detail in the complete paper show that the general pattern of the seedling is changed from the normal in the operated series in the direction of a higher proportion roots to hypocotyl (or to the whole plant). Further it appears that the operative procedure *per se* acted as a stimulus to the more efficient metabolic translocation of plastic food material from the cotyledons to the growing seedling than occurs in the normal plant under the described conditions of culture. Another noteworthy feature of the results was that the inherent growth rate, measured by r of the fitted logistic curves, was higher in the series from operated seeds than in the normal control plants. In association with this result it was found that the abscissa of the point of inflection of the growth curve—that is, the age of the seedling at the instant when the growth is most rapid per unit of time—increased with the weight of the seed planted. With some fluctuations due presumably to experimental and observational errors, the relationship between these two variables appears to be linear, and to follow the equation

$$I = 4.121 + .0580w,$$

where I denotes the point of inflection (in days of age) and w is weight of seed planted. The postponement of the period of most rapid growth as smaller and smaller amounts of the cotyledons are removed by operation was well marked, culminating in the control series at the end, which took the longest time of all to attain its maximum rate of growth.

For a more detailed presentation of the results and a discussion of their physiological implications the complete paper must be consulted.

[1] From the Department of Biology of the School of Hygiene and Public Health, Baltimore, Maryland.

[2] Pearl, R., *The Rate of Living*, New York (1928).

[3] Pearl, R., Winsor, A. A., and Miner, J. R., "The Growth of Seedlings of the Cantaloup *Cucumis melo*, in the Absence of Exogenous Food and Light," *Proc. Nat. Acad. Sci.*, **14**, 1–4 (1928).

[4] Pearl, R., Winsor, C. P., and White, F. B., "The Form of the Growth Curve of the Canteloup (*Cucumis melo*) under Field Conditions," *Ibid., Sci.*, **14**, 895–901 (1928).

[5] Shear, G. M., "Studies on Inanition in *Arachis* and *Phaseolus*," *Plant Physiol.*, **6**, 277–294 (1931).

AN X-RAY INDUCED CHROMOSOMAL TRANSLOCATION IN APOTETTIX EURYCEPHALUS HANCOCK (GROUSE LOCUSTS)[1,2,3]

BY ROBERT K. NABOURS AND W. R. B. ROBERTSON

DEPARTMENT OF ZOÖLOGY, KANSAS STATE COLLEGE AND DEPARTMENT OF ANATOMY, IOWA STATE UNIVERSITY

Communicated December 27, 1932

In the Department of Genetics, Carnegie Institution, 1929–1930, 128 males and 16 females of *Apotettix eurycephalus* Hancock, and 6 males and one female of *Paratettix texanus* Hancock (Grouse Locusts) were subjected to x-raying, ranging from 2000 to 8000 *R*-units, and at times when they appeared to be about ready to mate. Both parents of only two matings were treated. There were seven pairs of immediate, and several thousands of more remote, controls.

TABLE 1

PRODUCTIVITY OF X-RAYED INDIVIDUALS

R-UNITS	NUMBER OF INDIVIDUALS	NUMBER PRODUCTIVE	TOTAL OFFSPRING	AVERAGE NUMBER OF OFFSPRING
4000	11 males	7	30	4.3
6000	73 males	40	59	1.5
7000	34 males	1	1	1
8000	14 males	0	0	0
2000	2 females	2	15	7.5
4000	11 females	1	1	1
6000	2 females	0	0	0
4000	2 pairs	0	0	0
Controls	7 pairs	7 pairs	152	21.7

One of the 73 males of *A. eurycephalus* that had been treated with 6000 *R*-units, became the parent of five offspring, one male of which exhibited a broad white stripe along the median pronotum strikingly different from any pattern that might have been expected. This aberrant individual was lost during his third instar. The other 105 recorded progeny of the treated individuals were apparently phenotypically normal.

Eleven offspring of the x-rayed parents, *A. eurycephalus*, six at Cold Spring Harbor, and 5 of the 27 transported to the Kansas Station, gave progeny. Some of these have now (December 1, 1932) extended through 9 or 10 variously inbred generations, all apparently normal with the exception of those of the male described below.

An x-rayed male, of the composition *MZΘK/OTG*, one of the 73 treated with 6000 *R*-units, was mated to a female *RK/Z*. She was one of eight apparently regular offspring from a male treated with 4000 *R*-units. Of the 5 or 6 progeny, only 2, a male and a female, became large enough to be recorded. Phenotypically they were both *OTGRK*, one of the expected

CHART I CHROMOSOMAL TRANSLOCATION IN APOTETTIX EURYCEPHALUS

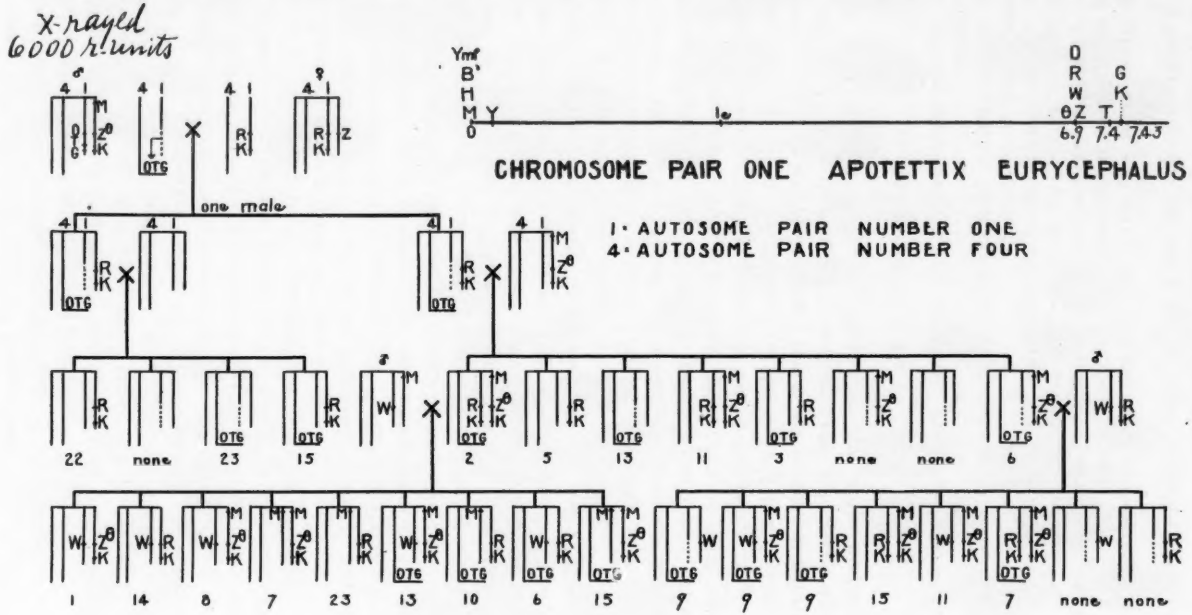

combinations. Only the male survived transportation to Kansas, and he was first mated to a "normal recessive" (+/+) female whose male parent had received 6000 *R*-units. They gave 60 recorded progeny. The same male was then mated to a female, $+/MZ\Theta K$, from untreated stock, and 41 resulting progeny were recorded. (Refer to the chart.) The progeny from this male, by both females, exhibited combinations of characteristics entirely unexpected, some of the individuals phenotypically including the characteristics *OTG* as well as *RK*. This result could not be accounted for on the basis of extensive past experience, as there had never been any crossing-over, between *O* and *R*, or *G* and *K*, in many thousands of pairings of the factors for these dominant color patterns (Nabours 1925, 1929, and there are many unpublished data).[4]

A further perusal of chart 1 reveals the factors *O*, *T* and *G*, linked, as having been translocated over to another entirely different linkage group, or pair of autosomal chromosomes. The new arrangement of the characteristics of the progeny of the sample matings shown in the chart clearly indicates that the factors *R* and *K* had not been the ones translocated, as could not be determined in the second generation. More than 9000 descendants of the x-rayed male have now (December 1, 1932) been recorded, and all support the supposition of the translocation of the portion of chromosome bearing the closely linked factors *O*, *T* and *G* from the original to an entirely new linkage group.

The chromosomes normal for a male *Apotettix eurycephalus* are represented by figure 1, the plate, a primary spermatocyte division at the stage of disjunction. Figures 2 and 3 are of spermatogonial and primary spermatocyte chromosomes from a grandson of the x-rayed male, one of the individuals included in the third group of F_2's in generation III of the chart. The cells, all direct descendants of the x-rayed male, of which these figures are camera lucida drawings, reveal a fragment attached to the proximal end of one of the number 4, medium sized, autosomes, figures 2–7. Some of them, figures 2–4, also show that one of the number 1,

---

DESCRIPTION OF PLATE 1

Figure 1. Primary spermatocyte, normal individual. Magnification lower than in remainder of figures.

Figure 2. Spermatogonium, "plus and minus" individual with "*OTG*" bearing fragment translocated from No. 1 to No. 4.

Figure 3. Primary spermatocyte of above individual.

Figure 4. Primary spermatocyte of another "plus and minus" individual.

Figure 5. Primary spermatocyte of "plus" individual. X-chromosome at upper left of figure seen at almost transverse section. No. 1's are normal.

Figure 6. Heterotetrad and normal No. 2 tetrad from another cell of above individual.

Figure 7. Primary spermatocyte from a second "plus" individual. Disjunction complete; X-chromosome much foreshortened; No. 1's normal.

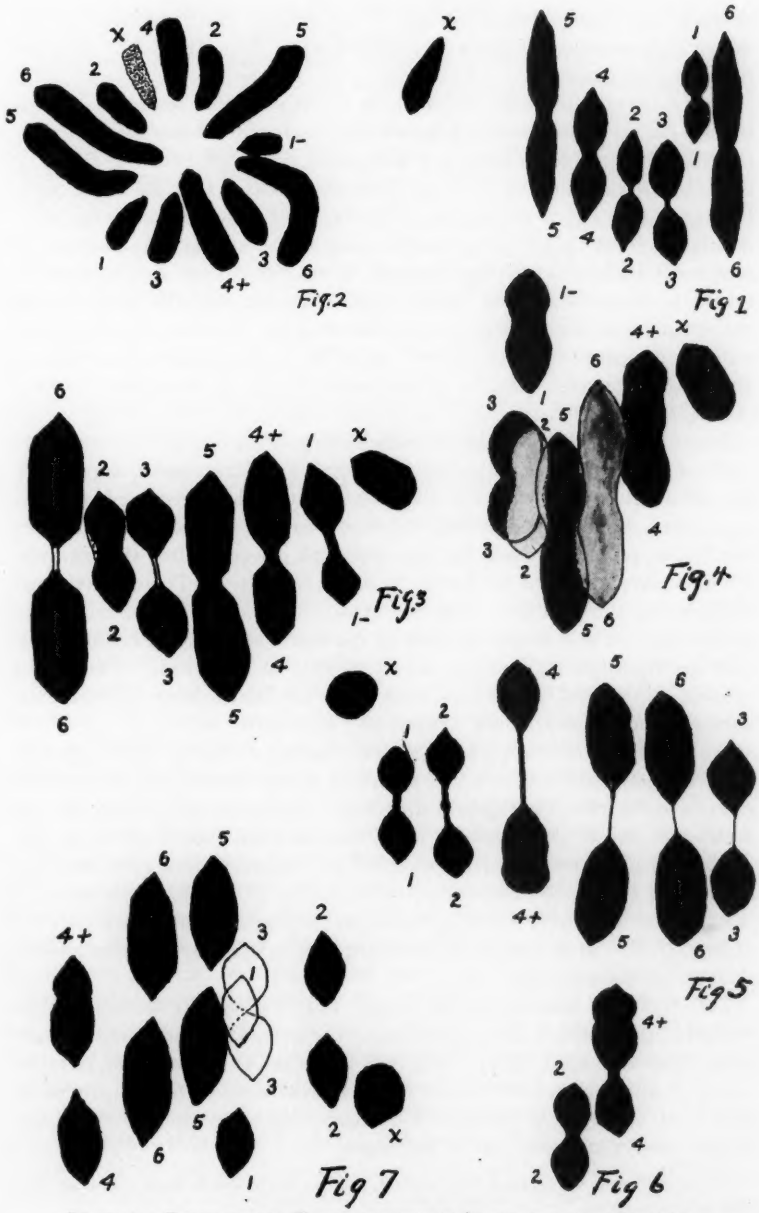

PLATE 1.—CHROMOSOMAL TRANSLOCATION IN APOTETTIX EURYCEPHALUS.
(For description see opposite page.)

smallest pair, has a deficiency, and it is therefore clearly marked as the donor chromosome. Figures 2, 3 and 4 show both the donor and the receptor chromosomes.

The receptor autosome, or diad, is slightly smaller than its normal homologue, as shown by the heterotetrad, and exhibits an indentation at its point of juncture with the translocated fragment (Figs. 2–7). The donor autosome, number 1, is also distinctly shorter than its homologue, but is not deficient to the extent of the fragment attached to the receptor, number 4 (Figs. 2–4). The translocation was probably to some extent reciprocal, with a larger piece donated to number 4 than was received in return by number 1. The translocated fragment probably must retain the spindle attachment fibre (or become attached to some other chromosome, or fragment, that has its fibres) as in Drosophila (Muller and Painter, 1929[5]; Dobzhansky, 1931[6]). These features will be considered further in a separate paper.

Zygotes in which this fragment was lacking, from one of the number 1, and not compensatingly attached to a number 4 chromosome, apparently did not develop, at least to the stage when they could be recorded (refer to the chart). Individuals having the translocation, but still duplicate for this fragment, are only a little less viable, 2.7 per cent, than the normals, the data showing 405 of the former to 436 of the latter. Those individuals triplicate for the translocated section of pair 1, fall about 10 per cent short of surviving as well as the normals to the stage, about third instar, when they are recorded, 2355 of the former to 2919 of the latter. These data support our general observation that many triplicates have difficulties in hatching and ecdyses, or are in some way deformed.

We are still in doubt as to the viability of those zygotes quadruplicate, triplicate and duplicate in which members of the fourth pair of chromosomes each carries the fragment attached. However, from 28 productive matings in which one parent, or both, had an equal chance of having the fourth pair of chromosomes duplicate for the fragment, none gave offspring all showing *OTG*. Furthermore, from a number of females, each carrying this translocated piece, the 19 parthenogenetic progeny were all without the pattern *OTG*. It is difficult to conceive of a better way of testing them than by parthenogenesis.

Thus we have learned, as one result, that the several factors for the conspicuous, dominant color patterns in *A. eurycephalus*, all in one linkage group (Nabours, 1925, 1929),[4] have been contained in the smallest, number 1, pair of autosomes, a fact about which we had hitherto been in complete ignorance. The newly established linkage group is attached to one of the middle sized, number 4, pair of autosomes.

[1] Paper 149 from the Zoölogy Department, Kansas Agricultural Experiment Station, Manhattan, Kansas.

[2] The experiment was aided by grants from the Carnegie Institution, and the HENRY FUND of the NATIONAL ACADEMY OF SCIENCES.

[3] The director and members of staff, and especially Dr. M. Demerec who shared greenhouse facilities, of the Department of Genetics of the Carnegie Institution, generously promoted the experiment.

[4] Nabours, Robert K., "Studies of Inheritance and Evolution in Orthoptera V," *Kans. Tech. Bull.*, **17**, 1–231 (1925); "The Genetics of the Tettigidae (Grouse Locusts)," *Bibliographia Genetica, Holland*. The Hague, Martinus Nijhoff, 27–104 (1929). Netherlands.

[5] Muller, H. J., and Painter, T. S., "Parallel Cytology and Genetics of Induced Translocations and Deletions in Drosophila," *Jour. Heredity*, **20**, 287–298 (1929).

[6] Dobzhansky, Th., "The Decrease of Crossing-Over Observed in Translocations, and Its Probable Explanation," *The Amer. Nat.*, **65**, 214–232 (1931).

THE GEOLOGY OF THE BEARTOOTH MOUNTAIN FRONT IN PARK COUNTY, WYOMING[1]

BY RICHARD V. HUGHES

GEOLOGICAL LABORATORY, JOHNS HOPKINS UNIVERSITY

Communicated December 27, 1932

Introduction.—(1) *Location.*—The Beartooth Mountain Range forms the Rocky Mountain front in southwestern Montana and extends about 12 miles across the state line into northwestern Wyoming. The Clark Fork River is usually considered to be the southern and southwestern boundary. The area described in this study includes about 175 square miles, approximately half of which lies east of the mountain front. Clark is the only postoffice within the area. It is located 40 miles northwest of Cody and about the same distance east of Yellowstone National Park.

(2) *Previous Work.*—Very little previous geological work has been done in this region. The earliest published account mentioning the geology of the mountain front was by Eldridge in 1894.[2] Fisher[3] briefly described the geology and water resources in 1906, and Woodruff[4] the coal resources in 1909. Dake[5] first mentioned overthrusting along the mountain front. Bevan[6] was the first to describe in detail the structure, peneplanation and orogenic history of the range. Alden[7] has studied the stream terraces and glaciation in relation to recent uplifting. And at present the Beartooth-Big Horn Mountains and Yellowstone National Park region is being studied by the Princeton Geological Research Group.[8]

(3) *Present Work.*—The area was mapped during the field season of 1931 in coöperation with the Princeton Geological Research Group. The stratigraphic section, areal distribution and attitude of the beds, and their structural relations were studied. All mapping north of the Clark Fork

TABLE 1

FORMATIONS EXPOSED ALONG THE BEARTOOTH MOUNTAIN FRONT—PARK COUNTY, WYOMING

PERIOD	EPOCH	GROUP AND FORMATION		THICKNESS (FEET)	CHARACTER
Quaternary	Recent and Pleistocene				Terrace gravel, glacial drift, alluvium.
Tertiary	Pliocene ?				Glacial boulders.
	Eocene	Fort Union formation		4300–6000	Lower part—very coarse to boulder conglomerate, usually poorly bedded and sorted; remainder chiefly argillaceous sandstones with many lenses of conglomerate and irregular sandy clays.
Cretaceous	Upper Cretaceous	Montana group	Bearpaw shales Judith River formation Claggett formation Eagle sandstone Telegraph Creek formation	1687–2300	Alternating marine and continental sandstones, shales and clays, mostly buff to rusty color. Sandstones very irregular along strike, fine-grained, often show cross-bedding. Some thin coals and carbonaceous matter present.
		Colorado group	Carlile and Niobrara shales	1962	Chiefly dark-colored to black fissile shale, top very sandy, many thin beds of concretions, some bentonitic zones.
			Frontier formation	628	Upper part alternating coarse rusty sandstones and conglomerates with shale, separated from a lower series of sandstones by a thick bed of laminated grayish shale.
			Mowry shales	417	Dark gray fissile shale and laminated gray sandstone, many beds of pure bentonite.
			Thermopolis shales	294	Dark laminated to fissile shale.
				2–7	Poorly cemented coarse sandstone, conglomerate with much organic material. "Muddy sand" of drillers.
				459	Black fissile shale with rusty sandy beds in lower part.
	Lower Cretaceous	Cloverly formation	Greybull sandstone member	74	Buff to rusty thin-bedded sandstone and dark shale.
				210	Bright variegated clays with a few indurated lenses.
				0–35	Dark pebble-conglomerate and sandstone.

		—Sharply channeled erosional unconformity—		
Cretaceous ?	?	Morrison formation	312	Two thick sandy clay-shales of dull colors separated by buff to rusty sandstone.
Jurassic	Upper Jurassic	Sundance formation	591	Chiefly gray to olive-drab shale with thin uniform limestones, dark gray sandstone at top.
		——Erosional unconformity ?——		
Triassic		Chugwater formation	775	Red shale, red clay and red fine-grained sandstone, more massive and indurated toward top. Much interbedded gypsum including, near the top, one bed 14′ thick.
		——Erosional unconformity ?——		
	Permian ?	Embar limestone	78	Impure limestones, gray, chiefly thin-bedded.
		—Apparently slight erosional unconformity—		
	Pennsylvanian	Tensleep sandstone	173	Light gray to buff, medium to coarse-grained, sandstone, cross-bedding common, several thin calcite veins and lenses of chert.
Carboniferous		—— Erosional unconformity ——		
		Amsden formation	176	Red and purple shales, impure limestones and sandstones with reddish quartzite at base.
	Mississippian	——Marked erosional unconformity——		
		Madison limestone	900	Limestone, chiefly gray to blue-gray, dense, fine-grained, thin-bedded to very massive, some chert and siliceous zones.
	Upper Devonian	Threeforks formation	67	Dark colored laminated shale, impure limestone and ripple-marked fine-grained sandstone.
		Erosional unconformity——		
Devonian			48	Buff limestone and massive dolomite.
	Middle Devonian	Jefferson dolomite — Upper member	294	Chiefly buff colored dolomite, fairly uniform in texture and bedding, some thin zones of limestone breccia.
		Basal member	75	Chiefly limestone and limestone-breccia, reddish color. Found only in channels cut in Bighorn dolomite.
		—— Marked erosional unconformity ——		
Ordovician	Upper Ordovician	Bighorn dolomite	476	Dolomite, very massive, uniform, fine-grained, buff, two very pure, ash-gray to white, thick limestone zones.
	Upper Cambrian	Gallatin limestone	448	Alternating beds of gray shale, thin-bedded limestone and limestone-pebble conglomerate, massive dolomite at base.
Cambrian	Middle Cambrian	Gros Ventre formation	646	Massive limestone-pebble conglomerate at top underlain by gray shales, laminated to fissile with impure limestones toward bottom.
		Flathead quartzite	48	Dark buff to brown sandstone and quartzite, chiefly thin-bedded with dark shale near the base.
Archean				Granites, gneiss, etc., perhaps sedimentary in part.

River and that part of the mountain front south of it was done by triangulation, using plane table and telescopic alidade. More detailed papers on the stratigraphy, structure and peneplanation of this region are in preparation.

Physiography.—The Beartooth Range consists essentially of an uplifted core of pre-Cambrian granitic and gneissic rocks flanked by sedimentary formations. The eastern slope is intersected by a fault plane which has commonly been considered an overthrust of considerable magnitude over much of its length. The frontal flank presents a bold front with steeply dipping to overturned sediments whose attitude is largely determined by drag along the fault. As viewed from the plains the bold front presents an unusually even sky-line which marks the eastern boundary of a very flat crest, usually termed the subsummit plateau. Its elevation ranges from 4000 to 5000 feet above the bordering plains and averages approximately 9500 feet above sea level. The southwestern side of the plateau is bounded for several miles by a large normal fault forming another prominent topographic feature. The whole area is drained by the Clark Fork River. West of the mountain front the river flows in a narrow canyon over 1000 feet deep in the vicinity of the Dilworth Bench. This narrow canyon is cut through a granitic floor which forms the wide "high-level valley" of the Clark Fork River. Little Rocky, Bennett and Line Creeks are the main tributaries.

Stratigraphy.—Erosion stripped the sedimentary cover most rapidly from the crest of the Beartooth uplift. The sediments are well exposed on both flanks and at the southern end of the uplift along the Clark Fork River. An excellent and easily accessible section of the Paleozoic beds is exposed within the Clark Fork Canyon where it cuts the mountain front. Also the lower part of the Mesozoic is well exposed near-by on the plainsward side of the front. The upper Mesozoic and Cenozoic sections have to be pieced together from plainsward exposures between Little Rocky and Line Creeks.

The oldest rocks within the area are granites, gneisses and schists, of different ages, but all pre-Cambrian. A study of these rocks has never been made in this area. Some of the gneisses and schists, very well exposed near the mountain front the Clark Fork River, Little Rocky and Bennett Creeks may be metamorphosed sediments as indicated by the excellent parallel banding. Pre-Cambrian sediments are known north of this area in the Stillwater region, Montana.[9] The mapped sedimentary rocks range from Middle Cambrian to Eocene with only the Silurian missing. Table 1 shows the age, general character and thickness of the formations, and the marked unconformities. The areal distribution is shown on the generalized map, figure 1.

The total thickness of the sediments is over 16,000 feet, of which the

larger percentage is shale and clay; sandstone and limestone are each represented by about 10 per cent of the total. The amounts of gypsum, bentonite and coal are quantitatively negligible.

Geological History.—During pre-Cambrian time the rocks of this region underwent strong tectonic disturbances and intense regional metamorphism followed by an enormously long period of erosion. The basal Cambrian sediments, of Middle Cambrian age, were deposited upon an almost

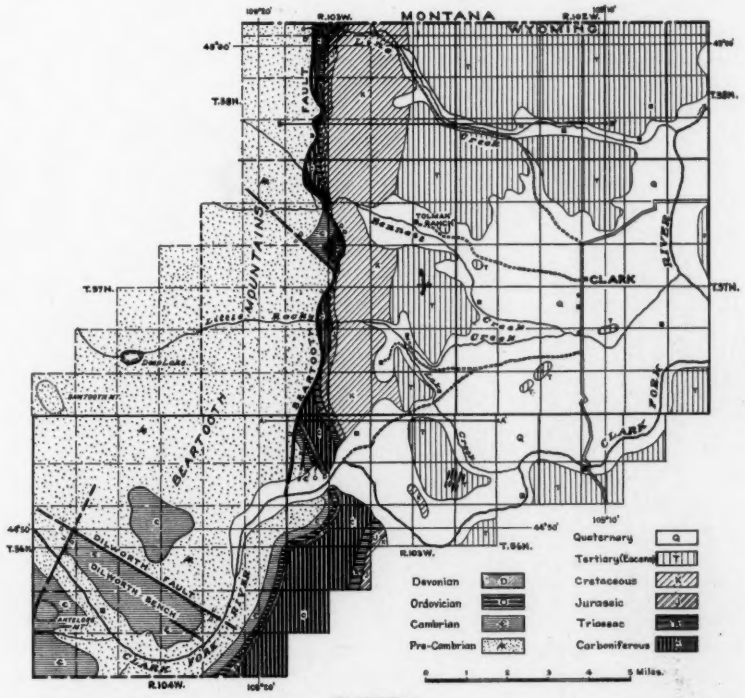

FIGURE 1

Generalized geological map of the Beartooth Mountain front in Park County, Wyoming.

featureless peneplain. Regional transgressions and regressions of the sea took place many times, especially during the Paleozoic. Gentle folding accompanied by small local thrusts apparently occurred during the late Paleozoic. Oscillatory warpings of regional extent are apparent also in the Mesozoic as shown by the diverse lithological character of the beds. The beginning of Upper Cretaceous volcanic activity is recorded in beds of early Colorado age. Regional uplifts and orogenic movements, probably first occurring to the west, are apparent in sediments of Montana age and

became strongly active in this region during the late Cretaceous and early Tertiary. The Beartooth Range was formed largely by uplift and faulting during these periods. Large regional uplifts have occurred since the Eocene and have continued, perhaps to a less degree, into Recent time.

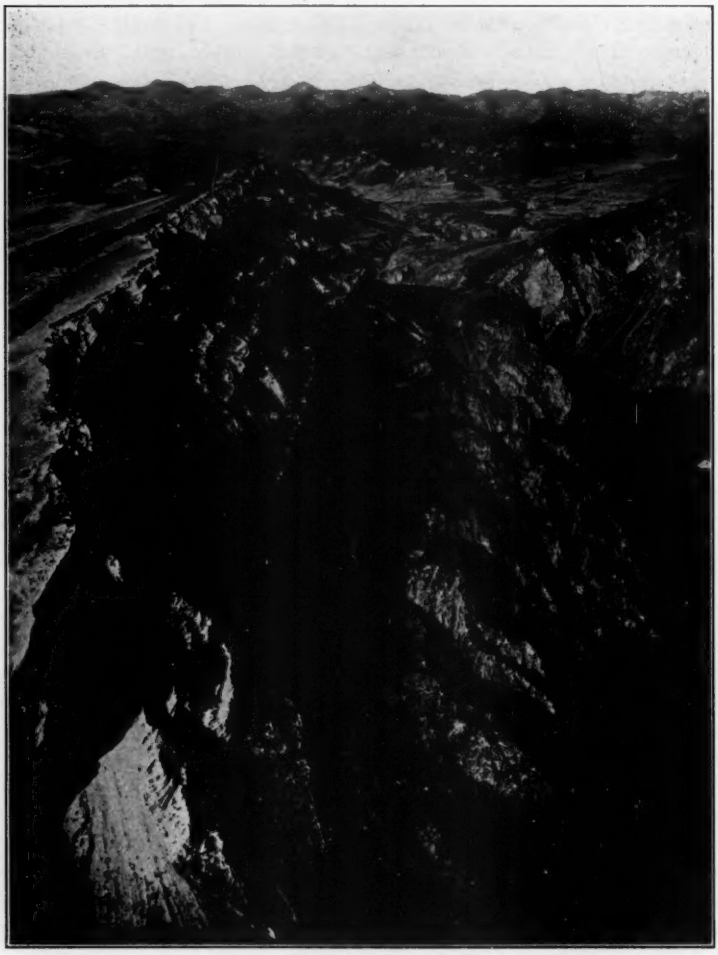

FIGURE 2

Aerial view of the Clark Fork Canyon looking W-SW taken from near the mountain front. The pre-Cambrian granitic erosion surface and the overlying Paleozoic sediments show clearly on the left (south side). (Reproduced by permission of C. J. Belden, Photo., Pitchfork, Wyo.)

Structural Geology.—(1) *General discussion.*—The earliest geological account mentioning the structure of the Beartooth Range was published by Eldridge in 1894.[10] At that time the Beartooth Range was included as a part of the Absaroka Mountains. The range consists essentially of a broad uplifted core of pre-Cambrian rocks flanked by sedimentary formations. The south end of the range has more the aspect of large, tilted, warped fault blocks than of a mountain range folded by direct compression.

A cross-section of the uplifted core shows very sharp flexing on the frontal (eastern) side which is modified by the Beartooth Fault. The crest is broad and very flat. The southwest flank shows a gentle dip toward the southwest and is broken for a distance of several miles by a normal SE-NW fault of approximately 2000 feet displacement, here called the Dilworth Fault, see figure 1. Other important faults of small displacement are on the north side of Antelope Mountain in a SW-NE direction, west of the Tolman Ranch in a SE-NW direction, and in two localities in the Tertiary formations at a distance of about $2^1/_2$ miles east from the mountain front.

An excellent cross-section of the southern end of the range is presented within the Clark Fork Canyon. This is well illustrated by the aerial view shown in figure 2. The Clark Fork River has cut around and through the southern nose of the uplift thus exposing over 1000 feet of pre-Cambrian rocks and nearly 3000 feet of the overlying sediments. The sharp bending of the pre-Cambrian rock surface and the Paleozoic sediments forming the east flank are well shown on the south side of the Clark Fork Canyon. The steep dip of the beds is dependent upon the amount of uplift and the tilting of the pre-Cambrian core, and is occasionally increased by fault movements. The dip of the beds becomes more gentle farther away from the mountains. The beds are usually horizontal or nearly so at a distance of about three miles.

The average dip of the Paleozoic rocks along the mountain front varies from 50°E. to slightly overturned. Near the Clark Fork River the Mesozoic beds are nearly vertical to overturned. The lower Mesozoic beds near the state line are overturned to low angles; whereas the upper Mesozoic beds dip eastward with equally low angles. The Tertiary beds are in a vertical position or nearly so along their basal contact on the west and become nearly horizontal within a short distance eastward. The topography of the front and the adjacent plainsward area, which has a width of about three miles, depends largely upon the attitude of the beds and their relative resistance to erosion.

The Beartooth Fault.—(1) *Previous interpretation.*—Faulting along the Beartooth Mountain front was first recognized by Wolff in 1884.[11] He drew a normal fault at the mountain front in his cross-section of the Rock Creek Coal Field, Montana. Eldridge[12] stated in a later report that fault-

ing did not extend south of the Montana-Wyoming state line. Fisher[13] mentions no faulting in this locality in his study of the Big Horn Basin. The importance of faulting and overthrusting in this part of Wyoming was first recognized by Dake.[14] He stated that there is a zone of thrust faults south of the Montana state line which brings pre-Cambrian granites in contact with overturned sedimentary formations as young as the Triassic.

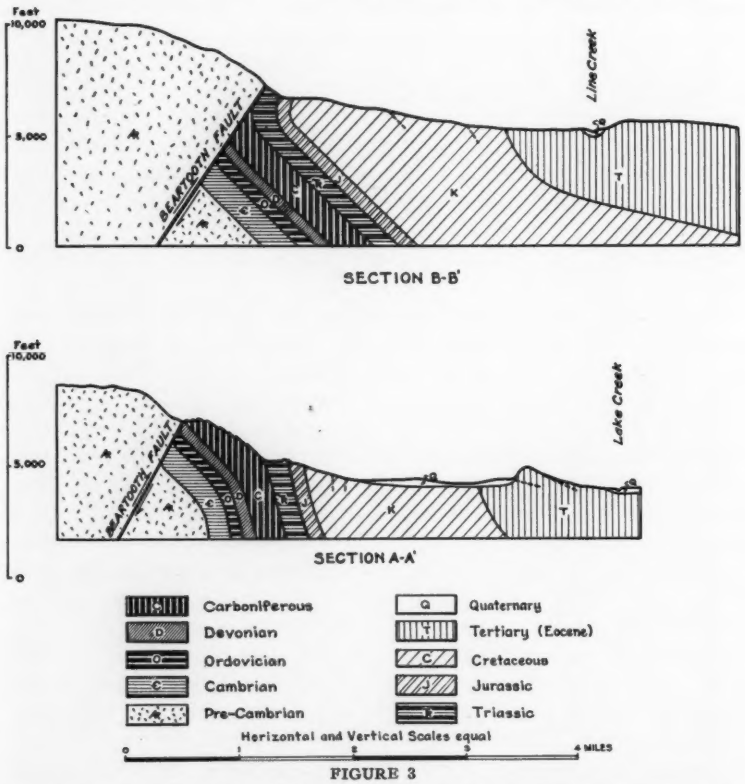

FIGURE 3

Structural sections in a W-E direction of the Beartooth Mountain front between the Montana state line and the Clark Fork River.

The faulting was considered as probably related to the same forces that produced the Heart Mountain Overthrust south of this area, but was not necessarily continuous with it as these fault planes were undoubtedly much steeper. Bevan[15] states that the plainsward front of the range is bounded throughout almost its entire length by the Beartooth Fault, which is an overthrust of considerable magnitude. It also appeared to him that

the Beartooth overthrust might be the northward extension of the Heart Mountain overthrust, and if not a direct continuation it was formed very probably during the same orogenic epoch. The maximum displacement was thought to be several miles. Many geologists have the impression from these papers that the Beartooth Fault *is* an overthrust of several miles. For instance Kober,[16] in describing Rocky Mountain front structure, states that the displacement is 7 miles in this locality.

2. *Present Interpretation.*—The general strike of the Beartooth Fault plane between the Montana state line and the Clark Fork River is almost due N-S. The slight irregularities shown on the generalized map, figure 1, are chiefly due to differences in elevation of its trace. Locally small breaks probably occur from one fault plane to another in "en echelon" manner. This is thought to occur particularly on both sides of Bennett Creek and near Line Creek.

Two sections across the mountain front are shown in figure 3. Section A-A' is taken 1 mile north of the Clark Fork River cutting through the saddle shown in figure 4. Section B-B' is $2^1/_2$ miles south of the Montana state line. It is taken a short distance south of the farthest exposure of Madison limestone which shows in figure 5. Both sections show the Beartooth Fault as a simple reverse fault. This brings up the question *is the Beartooth Fault an overthrust?* According to definition and usage an overthrust fault is a reverse fault with low angle or large hade.[17] A reverse fault is one where the hanging wall has been raised relatively to the footwall.[18] Based upon the field studies of 1931, that part of the Beartooth Fault between the Montana state line and the Clark Fork River can be explained better as a reverse fault. This interpretation is based upon: (1) the steep angle of the fault plane, and (2) the small displacement.

1. *The Steep Angle of the Fault Plane.*—The approximate angle of the Beartooth Fault plane is inferred from its surface trace, the attitude of the abutting footwall sediments, and a small paralleling fault on the north side of the Clark Fork River. A summary of these observations is given in table 2.

In this table the angles of the fault plane, according to the fault trace and the abutting footwall sediments, are relatively low only at and near-by Bennett Creek. If the paralleling fault plane is one of a series within a narrow fault zone the actual dip of the main fault plane should be approximately the same. If it represents slippage along a "feather joint" the dip of the main fault plane should be higher.[19] The dip of the abutting footwall sediments can readily be due to uplifting movements along the fault plane. The few low westward dips observed at the contact and a short distance from the fault plane can be explained by possible later movements within the sediments due to gravity or even later over-

thrusting from the west. Structural section *B-B'* is taken evidently very near the locality where Dake noted pre-Cambrian rocks in contact with Triassic beds which dipped under the granite at a low angle. The dip of the Madison limestone in this locality, however, where in contact with the granite, is not less than 60°W. and is as high as 85°W. Thus it seems reasonable to conclude that the angle of faulting is high.

TABLE 2

DIP OBSERVATIONS OF THE BEARTOOTH FAULT PLANE

	LOCATION OF OBSERVATIONS						
	NORTH SIDE OF CLARK FORK RIVER	SOUTH OF LITTLE ROCKY CREEK	NORTH OF LITTLE ROCKY CREEK	BENNETT CREEK	1 MILE NORTH OF BENNETT CREEK	1 1/2 MILES SOUTH OF LINE CREEK	LINE CREEK
Dip according to fault trace	> 60° W.	> 60° W.	> 45° W.	30° W. to 45° W.	> 45° W.	> 60° W.	
Dip of abutting footwall sediments	80° W. to Vertical	75° W. to Vertical	45° W. to 60° W.	35° W. to 60° W.	30° W. to 75° W.	60° W. to 85° W.	70° W.
Dip of paralleling fault plane	57° W.						

2. *The Small Displacements.*—The maximum displacement along a reverse fault with an assumed dip of 60° cutting the beds at the angles observed would be approximately 5000 feet. The measured thickness of the section to the highest beds now covered by granites (the Jurassic Sundance formation), also along a 60° reverse fault plane is 4600 feet. Thus the displacement along the Beartooth Fault plane hardly exceeded one mile. On the north side of the Clark Fork River the displacement is not more than a few hundred feet. And all fault movements appear to have died out somewhere between the north and south walls of the canyon.

The Dilworth Fault.—The normal fault bounding the Beartooth uplift for several miles on the southwest is here called the Dilworth Fault, a name used by prospectors in that locality. It was previously doubtfully described by Bevan as the Clark Fork Fault.[20] It strikes NW-SE and dips westward. The strike of the Flathead quartzite beds which were dragged along it is N.80°W. and the dip 70°W. to 80°W. The vertical displacement measures approximately 2000 feet by barometer along the Dilworth Bench, but it apparently dies out within the Clark Fork Canyon or in its south wall. Middle Cambrian Flathead quartzite and Gros Ventre beds uplifted by it are still present on the southern crest of the uplift. The Dilworth Fault forms the northeastern boundary of the Dilworth Bench and of the "high-level valley" of the Clark Fork River for several miles. Its trace northwestward was not followed beyond the limits of the map.

A small normal fault with upthrow on the southwest parallels the south end of the Dilworth Fault for a distance of about one mile. Its throw is less than 50 feet, but there is the aspect of a small graben between it and the Dilworth Fault.

Other Faults.—The fault shown on the north side of Antelope Mountain has a general SW-NE trend. The dip is nearly vertical and the displacement relatively small. The upthrow side is on the north. A short displacement toward the east on its south side is indicated by a sharp bend in the inner canyon of the Clark Fork River.

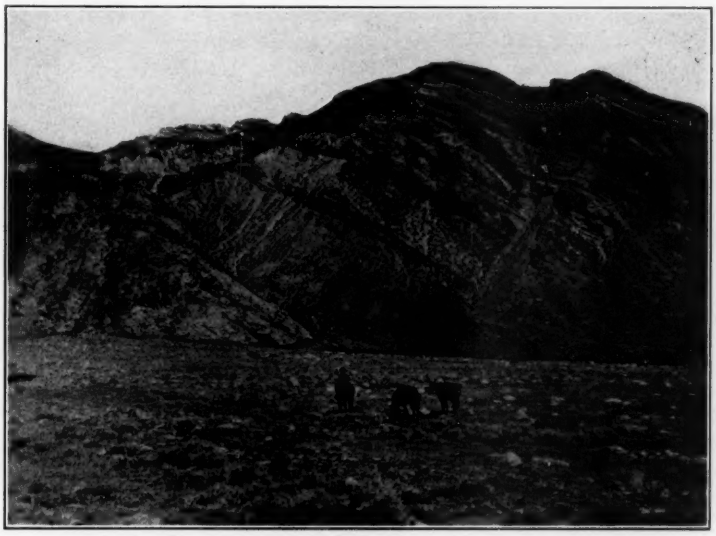

FIGURE 4

North side of the Clark Fork Canyon a short distance west of the mountain front. Pre-Cambrian rocks on left cut by several westward dipping fault planes. Paleozoic section including Madison limestone exposed on right.

The fault having a NW-SE trend located $2^1/_2$ miles west of the Tolman Ranch is only apparent by the presence of Middle Cambrian sediments abutting against granites. The upthrow side is on the southwest; displacement is relatively small. The dip is apparently very steep or perhaps vertical.

Small slippages have occurred along many of the joint planes not mapped for this study. The plainsward faults shown on the map, figure 1, are discussed under overthrusting.

Overthrusting.—One small plainsward overthrust and a zone of very

small eastward thrusts occur in the Tertiary (Eocene) formations at a distance of approximately $2^1/_2$ miles from the mountain front. The small overthrust $1^1/_2$ miles south of the Tolman Ranch is the most definite. It is a local feature not more than $^1/_2$ mile in length and results from a low angle break in a small overturned fold within the Eocene series. The maximum thrust was probably not over 100 feet. The dip of the thrust plane is 10°W.

The zone of surface thrusts is nearly opposite the mouth of the Clark

FIGURE 5

The Beartooth Mountain front looking south from the Montana state line. Nearly vertical beds of Madison limestone are seen on the frontal slope behind which is located the Beartooth Fault trace. Mesozoic beds dipping eastward to left of frontal slope.

Fork Canyon. Here the surface beds are too much disturbed for any measurements except strike readings which vary from N.12°E. to N.20°E. The thrust plane appears to be the upper surface of a more resistant series of sandstones within the formation dipping eastward with an angle of 9° to 15°.

These small surface thrusts may have been produced by gravity or less likely by the plainsward pressure of mountain glaciers. On the other hand it is entirely possible that the same forces which produced the Heart Mountain Overthrust were active to a small degree this far north. Other

evidences of overthrusting may have been eroded away. It is evident that these are the only features that can be related to the Heart Mountain Overthrust. In that case overthrusting was much later than the main uplifting movements of the Beartooth Range because the sediments involved are derived from near-by Middle Paleozoic rocks.

The Crest of the Beartooth Mountains.—The extensive plateaus of the Beartooth Mountains were interpreted a few years ago by Bevan[21] as remnants of two former peneplains formed by the action of wind and running water. The one of higher elevation was called the summit peneplain and the lower one the subsummitt peneplain. The subsummit peneplain is well represented south of the Montana-Wyoming state line. All the granitic area shown on the map, figure 1, north of the Clark Fork River and northeast of the Dilworth Fault may be considered a part of this extensive subsummit peneplain.

The broad even plateaus making up the southern end of Bevan's subsummit peneplain are here interpreted as remnants of a former plain, the exhumed marine plain upon which the basal Cambrian sediments were deposited.[22] The main factors leading to such an interpretation are:

1. The presence of a Middle Cambrian outlier at the south end of the Beartooth uplift.
2. The extreme evenness of the subsummit surface.
3. Erosion becomes practically halted by the beveled crystalline rocks.
4. The last 1000 to 2000 feet of uplift has occurred in comparatively recent time.

Acknowledgments.—The writer is indebted to Prof. W. T. Thom, Jr., of Princeton for the use of field equipment, the granting of material aid toward the work and the kind coöperation of the Princeton Geological Research Group. He is indebted also to Dr. Ernst Cloos and Dr. H. F. Reid of Johns Hopkins University for many suggestions in determining the structural relations of this area.

LITERATURE REFERRED TO IN TEXT

[1] Summary of a dissertation presented in partial fulfilment of the requirements for the degree of Doctor of Philosophy at Johns Hopkins University, 1933.

[2] Eldridge, G. H., "A Geological Reconnaissance in Northwestern Wyoming," *U. S. Geol. Survey, Bull.* **119** (1894).

[3] Fisher, Cassius A., "Geology and Water Resources of the Bighorn Basin, Wyoming," *U. S. Geol. Survey,* Prof. Paper 53 (1906).

[4] Woodruff, E. G., "Coal Fields of the Southwest Side of the Bighorn Basin, Wyoming," *U. S. Geol. Survey, Bull.* **341 B,** 200–219 (1909).

[5] Dake, Charles L., "The Hart Mountain Overthrust and Associated Structures in Park County, Wyoming," *Jour. Geology,* **26,** 45–55 (1918).

[6] Bevan, Arthur, "Summary of the Geology of the Beartooth Mountains, Montana," *Jour. Geology,* **31,** 441–465 (1923); "Rocky Mountain Peneplains Northeast of Yellowstone Park," *Jour. Geology,* **33,** 563–587 (1925).

[7] Alden, William C., "Physiography and Glacial Geology of Eastern Montana and Adjacent Areas," *U. S. Geol. Survey*, Prof. Paper 174 (1932).

[8] Bucher, Walter H., Thom, W. T., Jr., and Chamberlin, R. T., "Geologic Problems of the Beartooth-Bighorn Region," presented before the *Geol. Soc. America, 45th Annual Meeting* (1932).

[9] Peoples, Joe W., "Stillwater Igneous Complex, Montana," presented before the *Geol. Soc. America, 45th Annual Meeting* (1932).

[10] Eldridge, G. H., op. cit., 29–30.

[11] Eldridge, G. H., "Montana Coal Fields," *U. S. Tenth Census Report*, **15**, p. 755 and plate opposite (1890).

[12] Eldridge, G. H., "A Geological Reconnaissance in Northwestern Wyoming," *U. S. Geol. Survey, Bull.* **119**, 30 (1894).

[13] Fisher, Cassius A., op. cit., 37–39.

[14] Dake, Charles L., op. cit., 52–53.

[15] Bevan, Arthur, "Summary of the Geology of the Beartooth Mountains, Montana," *Jour. Geol.*, **31**, 457–461 (1923).

[16] Kober, L., *Der Bau der Erde, Gebrüder Borntraeger*, p. 321 (1928).

[17] Reid, H. F., and committee, "Report of the Committee on the Nomenclature of Faults," *Geol. Soc. America, Bull.* **24**, 179 (1913).

[18] Reid, H. F., and committee, op. cit., p. 177.

[19] Cloos, Ernst, " 'Feather Joints' as Indicators of the Direction of Movement on Faults, Thrusts, Joints and Magmatic Contacts," *Proc. Nat. Acad. Sci.*, **18**, 387–395 (1932).

[20] Bevan, Arthur, "Summary of the Geology of the Beartooth Mountains, Montana," *Jour. Geology*, **31**, 460–461 (1923).

[21] Bevan, Arthur, "Rocky Mountain Peneplains Northeast of Yellowstone Park," *Ibid.*, **33**, 563–587 (1925).

[22] Hughes, Richard V., "Peneplanation of the Beartooth Mountains in Wyoming," in press (1933).

ADDITIONAL LITERATURE, NOT MENTIONED IN TEXT

Alden, W. C., "Physiographic Development of the Northern Great Plains," *Geol. Soc. America, Bull.* **35**, 385–424 (1924).

Bevan, Arthur, "Rocky Mountain Front in Montana," *Geol. Soc. America, Bull.* **40**, 427–456 (1929); "Significance of Conglomerates in Interpreting the Mesozoic History of the Northern Rocky Mountains," *Ill. State Acad. Sci. Trans.*, **21**, 329–333 (1929).

Blackwelder, Eliot, "A Reconnaissance of the Phosphate Deposits in Western Wyoming," *U. S. Geol. Survey, Bull.* **470**, 452–481 (1911); "Post Cretaceous History of the Mountains of Central Western Wyoming," *Jour. Geology*, **23**, 97–117, 193–217, 307–340 (1915).

Condit, D. Dale, "Relations of the Embar and Chugwater Formations in Central Wyoming," *U. S. Geol. Survey*, Prof. Paper 98, 263–270 (1917); "Relations of the Late Paleozoic and Early Mesozoic Formations of Southwestern Montana and Adjacent Parts of Wyoming," *U. S. Geol. Survey*, Prof. Paper 120 (1918).

Dake, Charles L., "Glacial Features on the South Side of Beartooth Plateau, Wyoming," *Jour. Geology*, **27**, 128–131 (1919); "Episodes in Rocky Mountain Orogeny," *Am. Jour. Sci., 5th ser.*, **1**, 245–254 (1921).

Darton, N. H., "Geology of the Bighorn Mountains," *U. S. Geol. Survey*, Prof. Paper 51 (1906); "Paleozoic and Mesozoic of Central Wyoming," *Geol. Soc. America, Bull.* **19**, 403–470 (1908).

Hague, Arnold, "Absaroka Folio, Wyoming," *U. S. Geol. Survey, Folio* **52** (1899).

Hague, Arnold, Iddings, J. P., and Weed, W. H., "Geology of Yellowstone National Park," *U. S. Geol. Survey, Mon.* **32**, pt. 2 (1899).

Jepsen, Glenn L., "Stratigraphy and Paleontology of the Paleocene of Northeastern Park County, Wyoming," *Am. Philos. Soc. Proc.*, **69**, 463–528 (1930).

Hewett, D. F., "The Shoshone River Section, Wyoming," *U. S. Geol. Survey, Bull.* **541 C**, 89–113 (1914); "The Heart Mountain Overthrust, Wyoming," *Jour. Geology*, **28**, 536–557 (1920).

Knappen, R. S., and Moulton, G. F., "Geology and Mineral Resources of Parts of Carbon, Big Horn, Yellowstone and Stillwater Counties, Montana," *U. S. Geol. Survey, Bull.* **822**, 1–70 (1931).

Knowlton, F. H., "Flora of the Montana Formation," *U. S. Geol. Survey, Bull.* **163**, (1900).

Lee, Willis T., "Correlation of Geologic Formations Between East Central Colorado, Central Wyoming and Southern Montana," *U. S. Geol. Survey*, Prof. Paper 149 (1927).

Lovering, T. S., "The New World or Cooke City Mining District, Park County, Montana," *U. S. Geol. Survey, Bull.* **811 A** (1929).

Mansfield, G. R., "Geography, Geology and Mineral Resources of Part of Southeastern Idaho," *U. S. Geol. Survey*, Prof. Paper 152 (1927) (contains an excellent bibliography).

Thom, W. T., Jr., "The Relation of Deep-Seated Faults to the Surface Structural Features of Central Montana," *Am. Assoc. Petroleum Geologists, Bull.* **7**, 1–13 (1923).

Washburne, Chester W., "Coal Fields of the Northeast Side of the Bighorn Basin, Wyoming, and of Bridger, Montana," *U. S. Geol. Survey, Bull.* **341 B**, 165–199 (1909).

Willis, Bailey, "Rocky Mountain Structure," *Jour. Geology*, **33**, 272–277 (1925).

Woodruff, E. G., "The Red Lodge Coal Field, Montana," *U. S. Geol. Survey, Bull.* **341 A**, 92–107 (1909).

CHARACTERS OF ABELIAN GROUPS

BY R. E. A. C. PALEY[1] AND N. WIENER

DEPARTMENT OF MATHEMATICS, MASSACHUSETTS INSTITUTE OF TECHNOLOGY

Communicated January 14, 1933

1. In this note we give a preliminary account of some results which will be published in detail later.

The subject of group characters has been studied by Haar[2] who considers them in the case where the group is denumerable and by Peter and Weyl[3] who consider the characters of continuous groups. In this paper we are concerned only with Abelian groups, but, in this restricted field, we obtain results which are more complete than those of the two papers cited.

2. Let us consider an Abelian group G. We define a character of the group to be a function $\chi(A)$ of absolute value 1, defined on the elements A of G, such that, for any other transformation T of the group, we have

$$\chi(TA) = \chi(T)\chi(A) \qquad (1)$$

We observe that the product of two functions satisfying (1) is another

function also satisfying (1), so that the set of characters of the group form another group themselves. There is a certain sense in which it is possible to build up a duality between these two groups, and we shall discuss it later.

3. We begin our investigations by obtaining explicitly the functions which satisfy (1) in the case when the group G is denumerable. The simplest case is that in which the elements of G are all periodic, and, for that case, we will state our construction here, without proof. In the general case the procedure is essentially similar.

Suppose that the elements of G are written in a series

$$E, A_1, A_2, A_3, \ldots, A_n, \ldots, \tag{2}$$

where E denotes the identity transformation. We write $B_1 = A_1$, and suppose that n_1 is the least positive integer for which $A_1^{n_1} = E$. We strike out of the series (2) all the elements of the form $A_1^{m_1}$ $(1 \leqslant m_1 \leqslant n_1)$. Let B_2 be the first of the A's which remains. Let n_2 be the lowest integer for which $B_2^{n_2} = B_1^{k_{12}}$. We now strike out all the A's which are of the form $B_1^{m_1}B_2^{m_2}$ $(1 \leqslant m_1 \leqslant m_2,\ 1 \leqslant n_1 \leqslant n_2)$. If we continue indefinitely we have a series of equations of the form

$$\begin{aligned} B_1^{n_1} &= E, \\ B_2^{n_2} &= B_1^{k_{12}}, \\ B_3^{n_3} &= B_1^{k_{13}} B_2^{k_{23}}, \\ &\ldots\ldots \\ &\ldots\ldots \end{aligned}$$

and every member of G can be expressed as a finite product of B's.

We now construct a table in the following way. We first write 1 in a row by itself. Below it we write down all the solutions x_p of $x^{n_1} = 1$. Below each x_p we write down all the solutions $x_{p,q}$ of $x^{n_2} = x_p^{k_{12}}$. Below each $x_{p,q}$ we write all the solutions $x_{p,q,r}$ of $x^{n_3} = x_p^{k_{13}} x_{p,q}^{k_{23}}$, and so on.

We are now in a position to define our characters. For every infinite sequence $p, q, r, \ldots$ $(0 \leqslant p \leqslant n_1 - 1,\ 0 \leqslant q \leqslant n_2 - 1, \ldots)$ we define a character $\chi_{p,q,r}, \ldots$ to satisfy

$$\chi(B_1) = x_p,\ \chi(B_2) = x_{p,q},\ \chi(B_3) = x_{p,q,r}, \ldots$$

Then if

$$A = B_{m_1}^{\lambda_1} B_{m_2}^{\lambda_2} \ldots B_{m_k}^{\lambda_k},$$

we write

$$\chi(A) = \chi^{\lambda_1}(B_{m_1})\, \chi^{\lambda_2}(B_{m_2}) \ldots \chi^{\lambda_k}(B_{m_k}),$$

and we have defined χ for all A's.

4. Suppose now that G has more than $\aleph$ members. We show how to construct a set of denumerable Abelian groups $\{H\}$ such that every

member of G can be expressed uniquely as a finite product of members of the groups $\{H\}$. The simplest way to see this is the following. Suppose for simplicity that none of the elements of G are periodic and that they are arrayed in a well ordered series

$$E, A_1, A_2, \ldots \tag{3}$$

We write $B_1 = A_1$, and let H_1 consist of all the members of G which satisfy a relation of the form

$$A^m = B_1^n \neq E.$$

We delete from the series (3) all the members of H_1. Let B_2 be the first A which remains. H_2 is to consist now of all the A's which satisfy

$$A^m = B_2^n \neq E.$$

We delete from the series (3) all the members of G of the form

$$D_1^{n_1} D_2^{n_2}$$

where D_1 and D_2 belong to H_1 and H_2, respectively, and so on. We may proceed transfinitely, at each stage deleting all the finite products of members of groups H which we have already considered. If we now define a character χ for each of the groups $\{H\}$, we may define a character χ of G by means of the equation (1). Thus the set of characters of G can be completely determined.

We find ourself however in the position of having too many characters. Thus, for instance, if c denotes the number of the continuum and G has c members, then so has the set $\{H\}$. Each H has c characters, and thus G has $c^c > c$ characters. Our task therefore is to find some method of weeding out the superfluous characters. In certain cases we can do this.

5. Let us return to the denumerable case. Let G be the denumerable group and A its members, and let G^1 denote the group of characters χ. We observe that if A is fixed then $\chi(A)$ is a character of the group G^1 of elements χ, and from our point of view these (8) are the only interesting ones.

Our procedure is as follows. We build up a system of measure (by no means the only reasonable one) on the set χ in such a way that the functions $\chi(A)$ are the only measurable characters of G^1. All we have to do is to make a correspondence between the character $\chi_{p,q,r}, \ldots$ and the point

$$\frac{p}{n_1} + \frac{q}{n_1 n_2} + \frac{r}{n_1 n_2 n_3} + \ldots \tag{4}$$

of the line (0,1). This correspondence is $(1-1)$ except for a set of measure zero, and we now define the measure of a set of $\chi_{p,q,r}, \ldots$ to be that of the corresponding set of points (4). As we might expect, the system of

characters $\chi(A)$ form a complete normalized orthogonal system for the space χ, so that, if A, A' are different, the integral

$$\int_{G^1} \chi(A)\chi(A')d\chi$$

vanishes.

6. As an example of the procedure we have just defined we may give the case where G is defined by the equations $B_1^2 = E$, $B_2^2 = B_1$, $B_3^2 = B_2$, . . ., and consists of all finite products of the B's. Then the table defined above is

$$\begin{array}{cccccccccccccccc}
 & & & & & & & & 1 & & & & & & & \\
 & & & & 1 & & & & & & & & -1 & & & \\
 & & 1 & & & & -1 & & & & i & & & & -i & \\
1 & & -1 & & i & & -i & & \omega & & -\omega & & i\omega & & -i\omega & \\
 & & & & & & & & \cdots\cdots & & & & & & & \\
 & & & & & & & & \cdots\cdots & & & & & & &
\end{array} \tag{5}$$

where ω denotes $exp\left(\frac{1}{4}\pi i\right) = \sqrt{i}$. The group G^1 is then the dyadic group.

7. There are two directions in which we have succeeded in extending the ideas set out above. The first consists in extending tables of the form (5) so that they are unbounded to the right as well as downward. This enables us to define a system of measure on G^1 which is infinite instead of finite (we might, for instance, make a $(1-1)$ correspondence between the members of G^1 and the interval $(-\infty, \infty)$). The measurable characters G of G^1 are now no longer denumerable but of the order of the continuum. We can now build up a system of measure on G such that the elements of G^1 are the only measurable characters on G, and we have complete duality. The best known case is that in which both G and G^1 are the translation group on the infinite interval. One which is not continuous is that for which there is a correspondence between the elements of G (or G^1) and the finite binary numbers

$$\alpha_{-n}2^n + \alpha_{-n+1}2^{n-1} + \ldots + \alpha_0 + \alpha_1 2^{-1} + \alpha_2 2^{-2} + \ldots + \alpha_n 2^{-n} + \ldots, \tag{6}$$

where $\alpha = 0$ or 1 (we shall have to regard, for example, 1 and $2^{-1} + 2^{-2} + \ldots$ as distinct), and we define the product of (6) and

$$\beta_{-n}2^n + \beta_{-n+1}2^{n-1} + \ldots + \beta_0 + \beta_1 2^{-1} + \beta_2 2^{-2} + \ldots + \beta_n 2^{-n} + \ldots,$$

to be

$$\gamma_{-n}2^n + \gamma_{-n+1}2^{n-1} + \ldots + \gamma_0 + \gamma_1 2^{-1} + \gamma_2 2^{-2} + \ldots + \gamma_n 2^{-n} + \ldots,$$

where

$\gamma_r = \alpha_r + \beta_r \pmod 2 \quad (r = -n, -n+1, \ldots 0, 1, 2, \ldots n, \ldots).$

8. Our other generalization is that in which G^1 instead of being too large is too small. Suppose, for instance, that G^1 denotes Hilbert space $\sum x_n^2 < \infty$, and that the product of $\{x_n\}$ and $\{y_n\}$ is $\{x_n + y_n\}$. The most general character which is continuous is

$$exp\ \{2\pi i\ (\Sigma \lambda_n x_n)\},$$

where $\sum \lambda_n^2$ must converge. And, in this case, G also will be a Hilbert space. We use a very valuable theorem due to Banach[4] to show that if G^1 denotes a separable metric space of type[5] B, and if the fundamental operation is that of addition, then we can find a denumerable set of characters of G^1 such that, at any rate formally, every continuous character can be expressed as a finite or infinite product of powers of these fundamental characters.

[1] INTERNATIONAL RESEARCH FELLOW.

[2] A. Haar, "Über unendliche komutative Gruppen," *Math. Zeit.*, **33**, 129–159 (1931).

[3] F. Peter and H. Weyl, "Die Vollständigkeit der primitiven Darstellungen einer geschlossenen kontinuierlichen Gruppe," *Math. Ann.*, **97**, 737–755 (1927).

[4] S. Banach, *Théorie des opérations linéaires*, Warszawa, 1932.

[5] See, e.g., Banach, loc. cit., Chapter V.

GEOMETRY OF THE HEAT EQUATION: SECOND PAPER[1] THE THREE DEGENERATE TYPES OF LAPLACE, POISSON AND HELMHOLTZ

BY EDWARD KASNER

DEPARTMENT OF MATHEMATICS, COLUMBIA UNIVERSITY

Communicated January 4, 1933

1. The classical problem of the flow of heat by conduction in the plane suggests a corresponding problem in the differential geometry of families of plane curves. With a given flow of heat we associate a family of *heat curves:* namely, the complete set of ∞^2 isothermals throughout the flow; one curve for each temperature, for each value of the time. Then the physics of the flow is, at least in part, reflected in the geometry of the family of curves. We studied some simple questions of this geometry in our first paper, especially rectilinear and circular solutions.

Analytically, a flow of heat is described by giving the temperature v as a function of position and time

$$v = \varphi(x, y, t), \tag{1}$$

where the function φ must be a solution of Fourier's equation for the conduction of heat

$$\varphi_{xx} + \varphi_{yy} = \varphi_t, \quad \text{or} \quad \Delta\varphi = \varphi_t. \tag{2}$$

(We may assume that the coefficient of φ_t is unity by changing the unit of time, if necessary.) Then (1) is also the equation of the corresponding family of heat curves, if we think of v and t as parameters.

Heat families, then, are a class of two-parameter families of plane curves. In general they therefore contain ∞^2 distinct curves. But in certain cases the two parameters may combine so as to amount to just a single essential parameter. Then there are only ∞^1 curves, and the heat family is *degenerate*. Instead of varying with the time, the same ∞^1 curves serve as the lines of constant temperature all through the flow (though of course the temperature attached to a particular curve may change with the time).

For instance, degeneracy must occur when t is actually absent from φ, that is, in the case of steady flow. In fact (1) is then an ordinary *isothermal* (or Laplacian) family. But there are less obvious types, as stated below in Theorem II.

Clearly, if we wish to give a geometrical classification of families of heat curves, a first step must be to distinguish these special sets of ∞^1 curves from the general case. We therefore have the problem: *to determine all degenerate families of heat curves.*

Our main result is that there are three distinct types of degeneration of the Fourier heat equation. These may be connected with the equations of Laplace, Poisson and Helmholtz.

We first prove the following:

THEOREM I: A one-parameter system of curves can be identified with a degenerate family of heat curves if and only if its equation can be put in the form

$$g(x, y) = \text{const.}, \tag{3}$$

where g satisfies an equation of the form

$$\Delta g = ag + b, \tag{4}$$

where a and b are constants, and Δ denotes the Laplacian operator.

From this we deduce easily certain normal forms for all degenerate families:

THEOREM II: Any degenerate family (by means of a similitude transformation) can be given the equation $g(x, y) = \text{const.}$, where g is a solution of either $\Delta g = 0$, or $\Delta g = 1$, or $\Delta g = \pm g$.

THEOREM III: A family under one of these types cannot be under either of the others except that all three types include parallel straight lines and concentric circles (equations (11) and (12) below).

There are three distinct types of degenerate heat families:

TYPE I: *defined by the Laplace equation*

$$\Delta g = 0.$$

TYPE II: *defined by the special Poisson equation*

$$\Delta g = 1.$$

TYPE III: *defined by the Helmholtz-Pockels equation*

$$\Delta g = \pm g.$$

In the real domain the third type divides into two distinct cases,

$$\text{III}_1 : \Delta g = +g, \text{ and } \text{III}_2 : \Delta g = -g.$$

We have then more accurately four types in all, namely, I, II, III$_1$ and III$_2$.

It is obvious that the equation $\Delta g = -1$ is equivalent in the real domain to $\Delta g = +1$; hence type II requires no subdivision. On the other hand to reduce $\Delta g = -g$ to $\Delta g = +g$ one would have to replace x, y by ix, iy.

2. *Proofs.*—Assuming that φ is analytic in t, we can find the general solution of (2) explicitly in the form

$$\varphi = f + t\Delta f + \frac{t^2}{2!}\Delta^2 f + \ldots, \tag{5}$$

where $f(x, y)$ is an arbitrary function.[2]

The condition for (1) to represent only ∞^1 curves can be stated in this way: x and y must be separable from t within φ; that is,

$$\varphi(x, y, t) = \text{a function of } u \text{ and } t, \tag{6}$$

where u is some function of x and y.

It follows that each coefficient of (5) must separately be a function of u alone. It is no restriction to take $f(x, y)$ as equal to u. Hence $f(x,y)$ is to be determined by the infinite set of conditions

$$\Delta f = F(f), \tag{7$_1$}$$
$$\Delta^2 f = G(f), \tag{7$_2$}$$
$$\ldots\ldots \qquad \ldots$$

The function φ will then be found by substituting f into (5). The heat curves will be the one-parameter system

$$f(x, y) = \text{const.} \tag{8}$$

From (7$_1$) we obtain by differentiation

$$\Delta^2 f = F'F + (f_x^2 + f_y^2)F''. \tag{9}$$

Supposing first that $F'' \not\equiv 0$, we must have, according to (7$_2$),

$$f_x^2 + f_y^2 = \text{a function of } f. \tag{10}$$

But this is exactly the condition for (8) to represent a family of *parallel* curves. Then from (7$_1$) alone we readily prove that these parallel curves are either circles or straight lines. The solutions must be therefore the

parallel lines and concentric circles whose equations we determined in our first paper:

$$y = \beta(v, t), \quad \text{with} \quad \beta_v^2\beta_t - \beta_{vv} = 0, \tag{11}$$

$$x^2 + y^2 = \rho(v, t), \quad \text{with} \quad \rho_v^2(1 + \rho_t) - \rho\rho_{vv} = 0. \tag{12}$$

If $F'' \equiv 0$, we have from (7_1)

$$\Delta f = af + b. \tag{13}$$

Then (7_2), ... are all satisfied. Moreover, the f's for parallel lines and concentric circles can also be included in (13). Theorem I is therefore proved.

For an $f(x, y)$ obeying (13) it is easy to calculate from (5) the explicit form of φ, at least as far as t is concerned. If $a \neq 0$, (1) becomes (to some temperature scale)

$$v = (f + b/a)e^{at}; \tag{14_1}$$

and if $a = 0$, we find

$$v = f + bt. \tag{14_2}$$

THEOREM IV: *Hence in all possible degenerate cases (except of course the parallel straight lines* (11) *and the concentric circles* (12), *where t may appear in complicated algebraic or transcendental form), the temperature v is either independent of the time t, or else is linear in t, or else contains t exponentially. This corresponds to our three types I, II, III.*

The family (8) is not changed as a set of curves if we replace f by any function of itself. An f equivalent in this sense to any f under (13) will be found among the solutions of either $\Delta f = 0$, or $\Delta f = 1$, or $\Delta f = af$. If we allow magnification of the xy plane, the third equation can be specialized to $\Delta f = \pm f$, and we thus have Theorem II.

Furthermore, for any set of curves in two of the three types, we quickly prove that f obeys (10). As before, this means either parallel lines or concentric circles. Both of these families can actually be described by f's in all three classes, as Theorem III asserts, as follows.

Assuming our parallel straight lines horizontal we find that

y	= const.	Type I
$\frac{1}{2}y^2$	= const.	Type II
e^y	= const., $\sin y$ = const.	Types III_1 and III_2

are the proper forms.

For concentric circles about the origin the results are

$\log r$	= const.,	Type I
$\frac{1}{4}r^2$	= const.,	Type II
$I_0(r)$	= const., $J_0(r)$ = const.	Types III_1 and III_2

where J_0 is a standard Bessel function, and $I_0(r) \equiv J_0(ir)$, and r denotes the radius $(x^2 + y^2)^{1/2}$.

This completes the proof of Theorem III. Our three types of degeneration are therefore distinct in the sense that no family of ∞^1 curves, other than parallel straight lines and concentric circles, can belong to more than one type. *Any non-trivial degenerate heat family belongs to one and only one of the types defined by the Laplace, Poisson and Helmholtz equations.*

3. *Characterizations.*—We have found that all degenerate heat families can be classified under our three types I, II, III. This classification is analytic, depending on the form of the differential equations; but it can be translated, though not easily, into purely geometric form. The complete discussion is due to one of my students, Aaron Fialkow, who will publish a separate paper soon.[3]

For the first type, where the Laplace equation is obeyed, the result is known. Consider the given ∞^1 curves and the orthogonal trajectories, forming an ordinary isothermal net. At each point the sum of the rates of change of the curvatures with respect to the arcs is zero. *That is*

$$\frac{d\gamma}{ds} + \frac{d\gamma_1}{ds_1} = 0 \tag{15}$$

is the complete geometric equivalent of the Laplace equation

$$\varphi_{xx} + \varphi_{yy} = 0.$$

This property (15), since it involves first derivatives of curvatures, is geometrically of the third order. In can easily be restated in terms of osculating parabolas, or centers of curvature of evolutes. I have given another characterization, in terms of isogonal trajectories, in Math. Annalen, vol. 59, p. 352–354 (1904).

The fact that types II and III do not possess properties of third order, but do possess (individually) two properties of fourth order was established by the writer in his seminar of 1917. Fialkow finds these properties in explicit form and *proves for the first time their sufficiency.* Thus we have

THEOREM V: *While type I is characterized by one intrinsic geometric property of third order, namely* (15), *type II requires two (complicated) properties of fourth order, and the same is true of type III.*

Fialkow has shown that the following geometric property (involving both tangential and normal intrinsic derivatives)

$$\gamma_1\left(\frac{d^2\gamma}{ds^2} - \frac{d^2\gamma_1}{dn_1 ds_1}\right) + \left(\frac{d\gamma_1}{dn_1} - \gamma_1^2\right)\left(\frac{d\gamma}{ds} + \frac{d\gamma_1}{ds_1}\right) = 0 \tag{16}$$

characterizes the general class of equations $\Delta u = F(u)$, which includes our three types as particular species.

4. In a later paper I shall extend the main results of the first and second papers to three dimensions, that is, to families of heat surfaces.[4] There are no solutions with ∞^2 planes (in the real domain). The three dimensional equations of Laplace, Poisson and Helmholtz again control the degenerate solutions.

[1] See Kasner, "Geometry of the Heat Equation: First Paper," *Proc. Nat. Acad. Sci.*, **18**, p. 475 (June, 1932), and abstract in *Bull. Amer. Math. Soc.*, **23**, p. 302 (1917). The present paper can be read independently of the first. I wish to thank G. Comenetz for his assistance in writing out the papers.

[2] Theorem I can be proved without assuming analyticity. Such proofs were given in my seminar in 1916, and again this year in shorter form by G. Comenetz. Hence all the results of the present paper are valid if we assume merely continuity and existence of partial derivatives.

[3] See abstract in *Bull. Amer. Math. Soc.*, p. 803, Nov., 1932.

[4] See abstract in *Ibid.*, pp. 811–812, Nov., 1932.

THEORY OF ELASTIC SYSTEMS VIBRATING UNDER TRANSIENT IMPULSE WITH AN APPLICATION TO EARTHQUAKE-PROOF BUILDINGS

By M. Biot

Department of Aeronautics, California Institute of Technology

Communicated January 19, 1933

Vibrating Systems under Transient Impulse.—The following theory gives a method of evaluating the action of very random impulses on vibrating systems (i.e., effect of static on radio-circuits or earthquakes on buildings). In the following text, we will use the language of mechanics.

Consider a one-dimensional continuous elastic system without damping. The free oscillations are given by the solutions of the homogeneous integral equation[1]

$$y = \omega^2 \int_a^b \rho(\xi)\alpha(x\xi)y(\xi)d\xi.$$

Due to the nature of the kernel there exists an infinite number of characteristic values ω_i of ω and of characteristic functions y_i solutions of this equation. These functions give the shape of the free oscillations of the system. They are orthogonal and have an arbitrary amplitude. This amplitude may be fixed by the condition of normalization,

$$\int_a^b \rho(\xi)y_i^2(\xi)d\xi = 1.$$

We now suppose that certain external forces $f(x)$ are acting on the system,

these forces being expressed in such a way that the product of the displacement y by $f(x)$ represents the work done by this force. For example if $f(x)$ is a moment y will be the angle of rotation around the same axis as the moment at that point.

It can be easily proved that the statical deflection of the system is,

$$y = \sum \frac{C_i}{\omega_i^2} y_i$$

where C_i is the Fourier coefficient of the development of $\frac{f(x)}{\rho(x)}$ in a series of the orthogonal functions y_i,

$$\frac{f(x)}{\rho(x)} = \sum C_i y_i$$

hence

$$C_i = \int_a^b f(\xi) y_i(\xi) d\xi.$$

If the applied forces are variable with time and harmonic of the form $f(x)e^{i\omega t}$ the deflection is expressed by the expansion

$$y = \sum \frac{C_i y_i}{\omega_i^2} \frac{1}{1 - \omega^2/\omega_i^2} e^{i\omega t}. \qquad (2)$$

The amplitude is composed of each of the terms of the statical deformation (1) *multiplied by a resonance factor* $\frac{1}{1 - \omega^2/\omega_i^2}$.

The motion due to a sudden application of the forces is of the same type, and can be deduced immediately from the preceding harmonic solution.

By using Heaviside's expansion theorem we get,

$$y_a = \sum \frac{C_i y_i}{\omega_i^2} [1 - \cos \omega_i t]. \qquad (3)$$

The amplitude due to a sudden applied force $f(x)$ is composed of a series of oscillations each of which has an amplitude equal to twice the corresponding term of the statical deformation (1).

We will now investigate the action of varying forces of the type $f(x)\psi(t)$; these forces are supposed to start their action at the origin of time and to keep on during a finite time T.

Using the Heaviside method, and the indicial admittance (3), the motion after the impulse has disappeared is given by,

$$y_b = \int_0^T \frac{d}{dt} y_a(t-\tau).\psi(\tau)d\tau,$$

$$y_b = \sum \frac{C_i y_i}{\omega_i^2}\left\{\sin \omega_i t[\omega_i \int_0^T \psi(\tau)\cos \omega_i \tau d\tau] - \cos \omega_i t[\omega_i \int_0^T \psi(\tau)\sin \omega_i \tau d\tau]\right\}.$$

This motion is the superposition of free oscillations. Their respective amplitudes can be physically interpreted as follows:

Put
$$f_1(\nu) = \int_0^T \psi(\tau)\cos 2\pi\nu\tau \, d\tau$$

$$f_2(\nu) = \int_0^T \psi(\tau)\sin 2\pi\nu\tau \, d\tau$$

where ν is the frequency $\nu = \frac{\omega}{2\pi}$. The component free oscillations may then be written,

$$\frac{C_i y_i}{\omega_i^2} \cdot 2\pi\nu_i \sqrt{f_1^2(\nu_i) + f_2^2(\nu_i)}.$$

Now, according to the Fourier integral,

$$\psi(t) = 2\int_0^\infty f_1(\nu)\cos 2\pi\nu t d\nu + 2\int^\infty f_2(\nu)\sin 2\pi\nu t d\nu. \qquad (4)$$

This shows that the expression

$$F(\nu) = \sqrt{f_1^2(\nu) + f_2^2(\nu)}$$

may be considered as the "spectral intensity" curve of the impulse.

The amplitude of each free oscillation due to the transient impulse is

$$\frac{C_i y_i}{\omega_i^2} \cdot 2\pi\nu_i F(\nu_i). \qquad (5)$$

The expression $2\pi\nu F(\nu)$ is a dimensionless quantity that we will call "*reduced spectral intensity.*" We then have the following theorem: *When a transient impulse acts upon an undamped elastic system, the final motion results from the superposition of free oscillations each of which has an amplitude equal to the corresponding term $C_i y_i/\omega_i^2$ of the statical deformation* (1) *multiplied by the value of the reduced spectral intensity for the corresponding frequency.*

The advantage of this theorem is that for the calculation of the motion it replaces a complicated impulse by a spectral distribution which is always an analytical function of the frequency.

This theorem could also have been established by starting from (2)

and using directly the Fourier integral. We will apply this last method in order to generalize the theorem to the case of an elastic system with viscous damping whose motion is defined by the equation,

$$my + a\dot{y} + b^2y = A\psi(t). \tag{6}$$

The impulse is supposed to be given as before by the spectral distribution (4). Introducing a complex spectral distribution,

$$\varphi(\nu) = f_1(\nu) - if_2(\nu)$$

we may write,

$$\psi(t) = \int_{-\infty}^{+\infty} \varphi(\nu)e^{2\pi i\nu t}d\nu, \tag{7}$$

where according to the Fourier integral

$$\varphi(\nu) = \int_0^T \psi(\tau)e^{-2\pi i\nu t}d\tau.$$

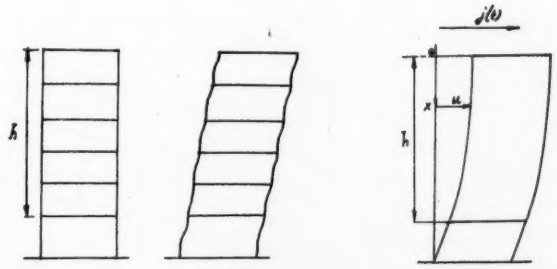

FIGURE 1

The function $\varphi(\nu)$ is holomorphic; its expansion in a power series is,

$$\varphi(\nu) = \sum \frac{A_n\nu^n}{n!}$$

where

$$A_n = (-2\pi i)^n \int_0^T t^n\psi(t)dt.$$

Calling M the largest value of $|\psi(t)|$ and $I(\nu)$ the coefficient of i in the variable ν considered from now on in the complex plane, we have

$$|\varphi(\nu)| < \frac{M}{2\pi T(\nu)}[e^{2\pi T(\nu)T} - 1].$$

This shows that for $t > T$, $|\varphi(\nu)e^{2\pi i\nu t}|$ has an upper limit.

Consider now the elastic system (6) under a harmonic impulse $Ae^{2\pi i\nu t}$, the corresponding motion is

$$x(t) = \frac{Ae^{2\pi i\nu t}}{8\pi^2\beta m}\left[\frac{1}{\nu - \nu_1} - \frac{1}{\nu - \nu_2}\right]. \tag{8}$$

The quantities ν_1 and ν_2 are complex frequencies

$$\nu_1 = \alpha i + \beta, \qquad \nu_2 = \alpha i - \beta.$$

The free oscillation of the system is damped and given by

$$e^{-2\pi\alpha t}\cos 2\pi\beta t.$$

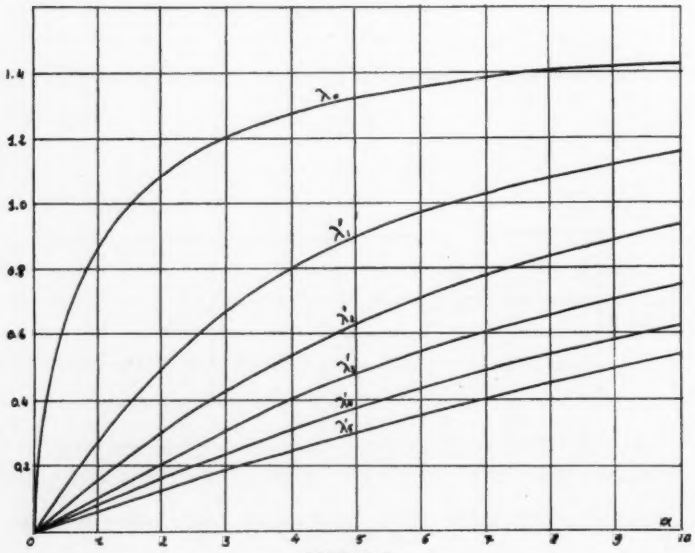

FIGURE 2

According to (7) and (8) the motion due to the impulse $A\psi(t)$ will be,

$$y(t) = \frac{A}{8\pi^2\beta m}\int_{-\infty}^{+\infty} \varphi(\nu)e^{2\pi i\nu t}\left[\frac{1}{\nu - \nu_1} - \frac{1}{\nu - \nu_2}\right]d\nu.$$

We have seen that $|F(\omega)e^{i\omega t}|$ has an upper limit, and by using then the method of contour integrals and residues, we find,

$$y(t) = \frac{A\pi i}{4\pi^2\beta m}\left[\varphi(\nu_1)e^{2\pi i\nu_1 t} - \varphi(\nu_2)e^{2\pi i\nu_2 t}\right].$$

At the time T when the impulse has ceased, the amplitude is,

$$|y(t)| = \frac{A}{4\pi^2\beta^2 m} 2\pi\beta \,|\varphi(\alpha i + \beta)|\, e^{-2\pi\alpha T}.$$

The quantity $\frac{A}{4\pi^2 m(\beta^2 + \alpha^2)}$ is the deflection for the static deformation due to a force A. *This last result generalizes formula* (5) *to the case of damping. We have to consider a complex frequency* $\alpha i + \beta$ *and the analytical prolongation* $\varphi(\alpha i + \beta)$ *of the spectral distribution* $\varphi(\nu)$ *of* $\psi(t)$.

Application to Earthquakes.[2]—The study of seismogram spectral distributions has not yet been made; it is, however, the author's opinion that this study would be of great importance for two reasons:

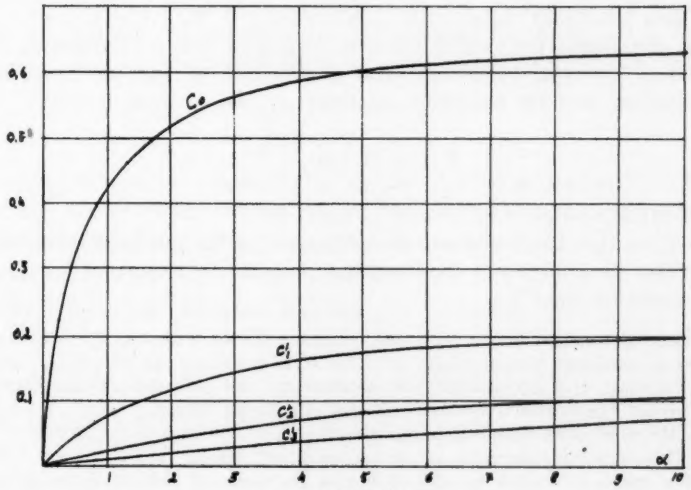

FIGURE 3

(1) The peaks of the spectral curves will reveal the presence of certain characteristic frequencies of the soil at given locations.

(2) By applying the preceding theorems the maximum effect of earthquakes on buildings will be easily evaluated by considering a spectral distribution having larger values than those deduced from known seismograms.

The theory has been applied to evaluate the effectiveness of the so-called "elastic first floor" in earthquake-proof buildings.

The building is supposed to have a simple frame, whose only possible deformation is shear (Fig. 1). All the stories except the first have a uniform mass and shear-rigidity. Call R the ratio of rigidity of the

first story to the rigidity of the second, $n + 1$ the number of stories and M the total mass of the n stories above the first one. Put $\alpha = Rn$.

The building is replaced by a continuous beam of same average properties.

The frequencies of the free oscillations are given by

$$\nu_K = \frac{\lambda_K}{2\pi t_0}$$

where t_0 is the time necessary for a shear wave to go from the second floor to the top, and λ_K are functions only of α given by $\lambda \nu g \lambda = \alpha$. The values of λ'_K are plotted in figure 2 with $\lambda_K = k\pi + \lambda'_K$.

Suppose that $j_0\psi(t)$ is the horizontal acceleration seismogram and that we have calculated the spectral intensity $F(\nu) = \sqrt{f_1^2(\nu) + f_2^2(\nu)}$ of $\psi(t)$. The earthquake produces a series of co-existing free oscillations in the building. A total horizontal shear is produced by each of these free oscillations, and the maximum amplitude of each of these shears is,

$$S = j_0 M C_K(\alpha) \frac{F(\nu_K)}{t_0}.$$

The values of $C_K(\alpha)$ are plotted in figure 3.

We see that the fundamental oscillation is by far the most dangerous, and that the influence of the elastic first floor is only important for values of α smaller than 3.

[1] See for instance, F. H. van den Dungen, *Cours de Technique des Vibrations*, Brussels, 1926, and "Les Problèmes Généraux de la Technique des Vibrations," *Mém. Sc. Physiques*, t. 4 (Paris, 1928); K. Hohenemser, *Die Methoden zur angenäherten Lösung von Eigenwertproblemen in der Elastokinetic* (Berlin, Springer, 1932). The function $\alpha(x, \xi)$ is called the influence function.

[2] This study was undertaken at the suggestion of Professor Th. von Kármán. The author wishes to express his appreciation of the continual interest Professor von Kármán and Professor R. R. Martel have taken in its progress.

A JORDAN SPACE CURVE WHICH BOUNDS NO FINITE SIMPLY CONNECTED AREA

BY JESSE DOUGLAS

DEPARTMENT OF MATHEMATICS, MASSACHUSETTS INSTITUTE OF TECHNOLOGY

Communicated January 11, 1933

The author, in collaboration with Ph. Franklin, has recently given a simple example of a Jordan space curve, in the form of a skew polygon of a denumerable infinity of sides, every surface bounded by which has infinite area.[1] Since then, I have found an even simpler and more striking example, which it is the purpose of the present note to communicate.

Description.—In a Cartesian xy-plane, take the segment of the x-axis between (3,0) and (4,0) as diameter, and construct the circle C_0. If this be subjected to a homothetic transformation from the origin O as pole and of ratio

$$\rho = \frac{1}{\sqrt{2}} < \frac{3}{4},$$

a circle C_1 is obtained whose disc is entirely external to that of C_0. By repeating the operation indefinitely, that is, effecting homothetic transformations from O of ratios

$$1, \rho, \rho^2, \ldots, \rho^n, \ldots$$

we obtain an infinite sequence of circles

$$C_0, C_1, C_2, \ldots, C_n, \ldots,$$

mutually external, and shrinking to the point O as limit.

The areas of these circles form a geometric progression of ratio $\rho^2 = \frac{1}{2}$, so that, since $C_0 = \frac{\pi}{4}$,

$$C_n = \left(\frac{1}{2}\right)^n \frac{\pi}{4},$$

or

$$2^n C_n = \frac{\pi}{4}. \qquad (1)$$

Next, let the entire configuration of circles be revolved about the y-axis. Then we obtain a nest of similar tori

$$T_0, T_1, T_2, \ldots, T_n, \ldots,$$

mutually external, and shrinking to the point O as limit.

Now take a thread (of infinite length) and wind it successively, and always in the same sense, once about T_0, twice about T_1, four times about $T_2, \ldots, 2^n$ times about $T_n, \ldots$. The thread is supposed to be pulled

taut between successive tori—for instance, in the form of a common external tangent to their circular sections by the same axial plane. The winding may be quite arbitrary, subject only to the condition that the thread shall not intersect itself. Since the thread remains, from a certain point on, within an arbitrarily small sphere about the point O as center, it is evident that this construction gives a Jordan arc going from (4,0,0) to (0,0,0)—being a one-one continuous image of a line segment, *end-points included*. If to this arc we adjoin the lower semi-circle in the xy-plane (supposed vertical) on the segment (0,0) to (4,0) as diameter, a Jordan space curve J is formed.

J is my example.

Proof.—For the proof that every simply connected surface bounded by J has infinite area, we need nothing more than the following lemma.

LEMMA. *If a closed contour links N times with a torus, the area of whose generating circle is C, then on every simply connected surface bounded by the contour, the torus intercepts an area at least equal to NC.*

The reader will probably be willing to accept this lemma as evident. A proof may be had by means of the formula

$$S = \int\int \sec \gamma d\sigma_m$$

for the area of any surface, where $d\sigma_m$ is the circular projection of an element $d\sigma$ of the surface on any plane through a certain fixed axis, and γ is the angle between the tangent plane to the surface and the axial plane through the point of contact. By circular projection, we mean using as projecting curves the circles produced by rotating space about the given axis.

If the axis of the torus recedes to infinity, the torus becomes a cylinder, circular projection becomes ordinary orthogonal projection and the above formula is the classic one for the area of a surface in rectangular coördinates.

To establish the lemma requires, besides the trivial remark $\sec \gamma \geqq 1$, only the obvious topological fact that every element $d\sigma_m$ of C corresponds to at least N elements $d\sigma$.

The condition of simple connectivity on the surface S is absolutely essential. If we form a Möbius strip from a rectangle in the usual way, making the construction so that the strip links with a given torus, then the boundary of the strip links twice with the torus, whereas the area of the strip intercepted by the torus is zero.

Now, let S denote any simply-connected surface bounded by J. Since the linking number of J with the torus T_n is $N = 2^n$, it follows by the lemma that the area of the portion of S intercepted by T is at least

$$2^n C_n = \frac{\pi}{4},$$

according to (1). But the number of tori is infinite, and they are mutually external; consequently

$$Area\ of\ S \geqq \frac{\pi}{4} + \frac{\pi}{4} + \ldots + \frac{\pi}{4} + \ldots,$$

or

$$Area\ of\ S = +\infty.$$

In my solution of the problem of Plateau,[2] I have shown that every Jordan curve is the boundary of a simply connected minimal surface M:

$$x_i = RF_i(w), \qquad \sum_{i=1}^{n} F_i'^2(w) = 0.$$

This applies to the present example J, where the area of M like that of every other simply connected surface bounded by J, is infinite. A good sense in which M still has the least area property, in spite of the area functional becoming identically infinite, was given by me in a previous paper.[3]

[1] "A Step-Polygon of a Denumerable Infinity of Sides Which Bounds No Finite Area," these PROCEEDINGS, **19**, 188–191 (1933).

[2] "Solution of the Problem of Plateau," *Trans. Amer. Math. Soc.*, **33**, No. 1, 263–321 (1931).

[3] "The Least Area Property of the Minimal Surface Determined by an Arbitrary Jordan Contour," these PROCEEDINGS, **17**, 211–216 (1931).

ON LACUNARY POWER SERIES

BY R. E. A. C. PALEY[1]

DEPARTMENT OF MATHEMATICS, MASSACHUSETTS INSTITUTE OF TECHNOLOGY

Communicated January 14, 1933

1. We consider a power series

$$\sum_{k=1}^{\infty} a_k z^{n_k}, \tag{1}$$

where $n_{k+1}/n_k \geq q > 1$ $(k = 1, 2, \ldots)$, the circle of convergence is supposed to be $|z| = 1$, and

$$\sum_{k=1}^{\infty} |a_k| = \infty. \tag{2}$$

I have proved the following theorem, which was suggested to me by Professor Zygmund.

THEOREM I. *If the condition* (2) *is satisfied and* $a_n \longrightarrow 0$, *then the series* (1) *will converge to any arbitrary complex number in an everywhere dense set of points on the circle of convergence.*

2. It seems plausible that the following associated theorem is also true, but so far neither Professor Zygmund nor I have succeeded in proving it.

THEOREM II. *If the condition* (2) *is satisfied, then the series* (1) *will converge to any arbitrary complex number in at least one interior point of the circle of convergence.*

3. We observe in passing that Theorem I assures us that the function (1) assumes inside the circle values arbitrarily near to any assigned number, so that the set of exceptional values is at any rate nowhere dense.

[1] INTERNATIONAL RESEARCH FELLOW and Research Fellow, Harvard University.

A MATRIX KNOT INVARIANT

BY J. W. ALEXANDER

DEPARTMENT OF MATHEMATICS, PRINCETON UNIVERSITY

Communicated January 11, 1933

Let K be any smooth, closed curve in a Euclidean 3-space R. Then the curve K determines an infinitely sheeted covering space R_∞ spread over the space R and such that as we go around the curve K we traverse the sheets of R_∞ in cyclical order. The topological invariants of the space R_∞ are, obviously, functions of the knot type of the curve K. We shall fix our attention, more particularly, on the group G formed by the one-cycles of R_∞ that are independent with respect to homologies.

Now, the homology group G cannot, in general, be generated by a finite number of cycles, in the restricted sense of the word "generate." Let us, however, introduce an operator x and form the ring Ξ consisting of all *finite* sums of the form

$$\sum_i a_i x^i, \qquad (i = 0, \pm 1, \pm 2, \ldots),$$

where the coefficients a_i are arbitrary integers. Then, it can be shown that there is a finite set of one-cycles,

$$C_i, \qquad (i = 1, 2, \ldots, s),$$

of the covering space R_∞ such that every cycle C of R_∞ is homologous to a linear combination of the cycles C_i,

$$C \sim \sum_i \alpha_i C_i,$$

with coefficients α_i in the ring Ξ. Moreover, there is always a finite set of homologies,

$$A_j = \sum_i \alpha_{ij} C_i \sim 0, \tag{1}$$

such that every homology among the C_i's is of the form

$$\sum_j \beta_j A_j = \sum_{i,j} \beta_j \alpha_{ij} C_i \sim 0,$$

where the coefficients β_j are also in the ring Ξ.[1] The geometrical significance of the operator x is as follows. If C is any curve of the covering space R_∞ the curves $x^i C$, $(i = 0, \pm 1, \pm 2, \pm 3, \ldots)$, all lie directly "over" or "under" C but in different sheets of R_∞.

A fundamental set of homologies (1) can be read off, by inspection, from the diagram of the knot K. It turns out that the coefficients α_{ij} are linear in x,

$$\alpha_{ij} = a_{ij} x + b_{ij}, \qquad (a_{ij}, b_{ij} \text{ integers}),$$

and that the matrix of the coefficients α_{ij} is a square matrix, such that its determinant reduces to unity when we write $x = 1$. We shall denote the matrix of the α_{ij}'s by

$$L(x) = M + xN, \tag{2}$$

where M and N are square matrices with integer elements. It can be shown that if the knot K is transformed into a knot K' isotopic to K then the matrix $L(x)$ goes over into a matrix $L'(x)$ ϵ-equivalent to $L(x)$.[2] However, necessary and sufficient conditions for the ϵ-equivalence of two matrices are not known, so that we are unable, as yet, to make the fullest possible use of the matrix $L(x)$. We propose, in this note, to translate the problem of the ϵ-equivalence of two knot matrices into a more manageable form.

Suppose the determinant of N in (2) is equal to zero. Then, by elementary transformations on the rows of $L(x)$ we can reduce $L(x)$ to such a form that all the elements in the last row of N are zero. Moreover, by elementary transformations on the columns of $L(x)$ we can further reduce $L(x)$ until all the elements in the last row of M are zero, with the exception of the very last one of all which must reduce to ± 1, since the determinant of $L(1)$ is unity. The last row of $L(x)$ will now represent an homology

$$\pm C'_s \sim 0,$$

in terms of a new set of generators C'_i. We may, therefore, strike out the last row and column of $L(x)$, since this is equivalent to suppressing the redundant generator C'_s. A similar reduction may be carried out if

the determinant of M is equal to zero, as we shall, in this case, be led to an homology

$$\pm x\, C_s'' \sim 0,$$

whence, again, the generator C_s'' corresponding to the last column of the transformed matrix $L(x)$ will be redundant. We may, thus, keep on reducing the order of the matrix $L(x)$ until we reach the point where the determinants of M and N are both different from zero. The determinant of $L(1)$ will, obviously, be ± 1. We shall make it $+1$ by changing the signs of one row, if necessary.

Next, let us make the substitution $\lambda = x - 1$ in the right-hand member of (2). The matrix $L(x)$ will then go over into

$$J + \lambda N, \qquad (J = M + N), \tag{3}$$

where J is a matrix of determinant unity. By elementary transformations on the rows of the matrix (3) we shall reduce this matrix to the form

$$1 + \lambda A, \tag{4}$$

where 1 now represents the unit matrix. It is easy to prove that if K and K' are two isotopic knots then the matrices A and A' corresponding to K and K', respectively, are related in the following manner:

$$A' = P\, A\, P^{-1}, \tag{5}$$

where P is a square matrix with integer elements and of determinant ± 1. In other words, every invariant of A under the group of all transformations of type (5) must be a knot invariant. Suppose, for example, we form an arbitrary polynomial B in the matrix A,

$$B = a_0 + a_1 A + a_2 A^2 + \ldots + a_n A^n,$$

where the coefficients a_i represent diagonal matrices with integer elements a_i along their main diagonals. Then the elementary divisors of B will all be invariants of the knot K. For the special case where we write

$$B = (A - 1)^n - A^n, \qquad (n = 2, 3, 4, \ldots),$$

these elementary divisors will reduce to the coefficients of torsion of the n-sheeted covering space R_n with the knot as branch curve of order $n - 1$. The characteristic polynomial $\varphi(\lambda)$ of A is, obviously, the "x-polynomial" of the knot, except for the change of parameter $\lambda = x - 1$.

Many other invariants of the matrix A suggest themselves, but the arithmetical problem of finding a complete set of invariants of A under all transformations of the group (5) appears to be as yet unsolved. We

shall investigate the properties of the matrix A in greater detail in a paper which will appear shortly in the Annals of Mathematics.

[1] "Topological Invariants of Knots and Links," *Trans. Amer. Math. Soc.*, **30**, 275–306 (1928). See also Reidemeister's *Knotentheorie*, Springer, 1932.

[2] Loc. cit.

[3] Loc. cit.